CHALMERS
UNIVERSITY OF TECHNOLOGY

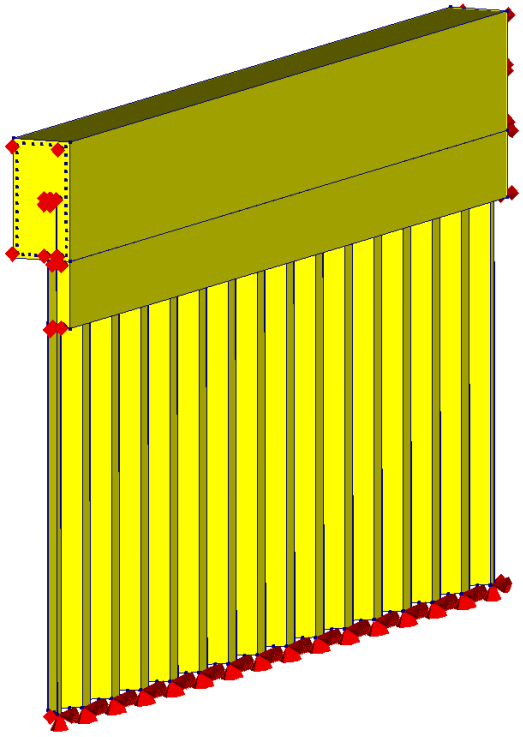

Advanced Finite Element Analysis of Fiber Reinforced Capping Beams

A study to evaluate if fiber reinforced concrete could be used to ease the production and increase the durability of capping beams

Master's Thesis in Structural Engineering and Building Technology

Jesper Bokinge
Nils Janestad

Department of Architecture and Civil Engineering

CHALMERS UNIVERSITY OF TECHNOLOGY
Gothenburg, Sweden 2021
www.chalmers.se

Master's thesis 2021

Advanced Finite Element Analysis of Fiber Reinforced Capping Beams

A study to evaluate if fiber reinforced concrete could be used to ease the production and increase the durability of capping beams

Jesper Bokinge
Nils Janestad

CHALMERS
UNIVERSITY OF TECHNOLOGY

Department of Architecture and Civil Engineering
Division of Structural Engineering
Concrete Structures
Chalmers University of Technology
Gothenburg, Sweden 2021

Advanced Finite Element Analysis of Fiber Reinforced Capping Beams
A study to evaluate if fiber reinforced concrete could be used to ease the production and increase the durability of capping beams
Jesper Bokinge
Nils Janestad

Supervisors: Ignasi Fernandez, Department of Architecture and Civil Engineering
Hadi Mazaheripour, Ramboll
Examiner: Ignasi Fernandez, Department of Architecture and Civil Engineering

Master's Thesis 2021
Department of Architecture and Civil Engineering
Division of Structural Engineering
Concrete Structures
Chalmers University of Technology
SE-412 96 Gothenburg
Telephone +46 (0)31 772 1000

Cover: The geometry of a capping beam in the finite element software Diana.

Gothenburg, Sweden 2021

Advanced Finite Element Analysis of Fiber Reinforced Capping Beams
A study to evaluate if fiber reinforced concrete could be used to ease the production and increase the durability of capping beams
Jesper Bokinge
Nils Janestad
Department of Architecture and Civil Engineering
Chalmers University of Technology

Abstract

Marine and port structures are often built using reinforced concrete and steel. As these structures generally are designed for aggressive environments, it is needed to use dense reinforcement arrangements in order to minimize the crack widths in concrete elements. This will often result in difficulties during production and heavy workloads. It is therefore of great interest within the industry to investigate solutions that may increase the durability and ease the production of quay structures, such as the common solution of a concrete capping beam on a sheet pile wall. In this type of structure the concrete capping beam mainly serves as a stiff tip at the top of the wall which distributes loads uniformly to the sheet piles. The concrete capping beam can be extended into the water in order to protect sheet piles from corrosion in the tidal zone. This extended part of the beam is sometimes referred to as the capping beam extension. The aim of this thesis has been to investigate if fiber reinforced concrete can be used for replacing conventional reinforcement in the capping beam extension for a simplified production procedure and increased durability. Furthermore, the structural behaviour of the capping beam has been investigated and a secondary aim has been to investigate if the structure has beam behaviour.

A case study was performed where a capping beam from an actual project was chosen for finite element modelling, verifying the performance of the structure with the proposed design as well as investigating its behaviour. The results are showing that only a small part of the capping beam possesses beam behaviour and is active under loading. Results from the FE-model are further showing that fiber reinforcement could be used for replacing reinforcement bars in the capping beam extension, while the proposed design is not allowed according to the current guidelines in Sweden.

Keywords: capping beam, DIANA FEA, capping beam extension, fiber reinforced concrete, FRC, corrosion

Acknowledgements

During the spring of 2021, this master thesis was conducted at Chalmers University of Technology in collaboration with Ramboll Sverige.
We want to thank our supervisor at Ramboll, Hadi Mazaheripour, for excellent guidance throughout this project. We also would like to thank Ignasi Fernandez for taking on this project as both our examiner and supervisor.

Jesper Bokinge & Nils Janestad, Göteborg, June 2021

Contents

1

Introduction

Marine and port structures are often built using concrete and steel. As these structures are usually exposed to sea water, corrosion of steel elements is a common problem resulting in degradation of the structures, reducing their safety and performance. In order to achieve the expected lifetime of these structures, large cover thicknesses must be used along with dense reinforcement layouts in order to control the cracking process, resulting in heavy workloads during production and an extensive material use. Due to this there is a strong interest within the industry to investigate solutions that could improve production, limit the material use to a minimum and improve the safety of such structures.

1.1 Background

A common solution used in quay structures consists of a sheet pile wall tied back by anchors with a concrete cap along its tip, see Figure 1.1. The concrete cap is often referred to as a capping beam and it mainly serves as a stiff tip at the top of the wall which distributes loads uniformly to the sheet piles. Furthermore, the concrete beam can be extended downwards into the water in order to cover the steel sheet piles from corrosion in the tidal zone, part RC2 in Figure 1.1, which in this project is referred to as the capping beam extension. However, installation of the capping beam extension complicates the production since this part needs to be cast under water.

As port structures generally are designed for aggressive environments, it is needed to use a large cover thickness, as well as to minimize the crack widths in designed concrete elements, this leads to heavy workloads and difficulties during production due to dense reinforcement arrangements. Despite such measures it has been shown through numerous field investigations in Norway that berth structures often suffer severe uncontrolled reinforcement corrosion, threatening the performance as well as the safety of the structures, indicating that the minimum requirements with regard to durability in some concrete codes are not sufficient for this type of environment (Carl A. Thoresen, 2010). Therefore it is of great interest within the industry to investigate new solutions coupling ease in production and increased durability.

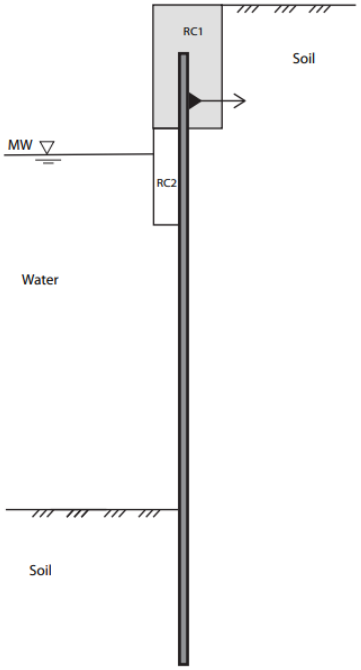

Figure 1.1: *Principal sketch of studied quay structure, RC1 is indicating the capping beam and RC2 is the capping beam extension.*

A possible solution to overcome these problems would be to use fiber reinforced concrete as means for cracking control and thus reducing the amount of steel reinforcement (Minelli et al., 2011). Using this concept can reduce the risk of corrosion of reinforcement as well as drastically simplifying the production of the structure. The used fiber could be synthetic fiber or a steel fiber since a lot of research has shown that steel fibers are not prone to corrosion if crack widths are limited (Bentur and Mindess, 2006). In order to verify that this alternative design could be used it is needed to show by calculations that the fiber reinforced structure possesses sufficient strength as well as its location of cracks. A critical part of the structure is the connection between the sheet pile and the concrete which must be investigated in order to see if shear connectors are needed. In Figure 1.2 the production of a capping beam is shown.

Furthermore, the capping beam is a composite element consisting of both the sheet pile and reinforced concrete. The actual behaviour of this type of structure when taking the sheet pile wall into account is not known and the research on it is very limited. A typical way of designing this type of structure is to assume that the capping beam acts as a simply supported continuous beam supported by the anchors. Not taking the influence of the wall into account and assuming that the concrete cap acts as a beam element in design might result in a conservative design and an unnecessarily high material use. It is therefore of interest to investigate the actual structural behaviour of the composite structure and compare the results of such analysis with obtained results from assuming beam behaviour.

Figure 1.2: *A capping beam on under construction (*PEAB*, 2021)*

1.2 Aim

The intended outcome of the thesis is to find a concept for an alternative design of the capping beam used in quay structures, by casting the capping beam extensions in fibre reinforced concrete instead of using traditional reinforced concrete, yielding a more durable structure with less risk of issues with corrosion and simpler production. The proposed concept is illustrated in Figure 1.3. The thesis also focuses on verifying the accuracy of the commonly used design assumptions and to investigate its actual structural behaviour.

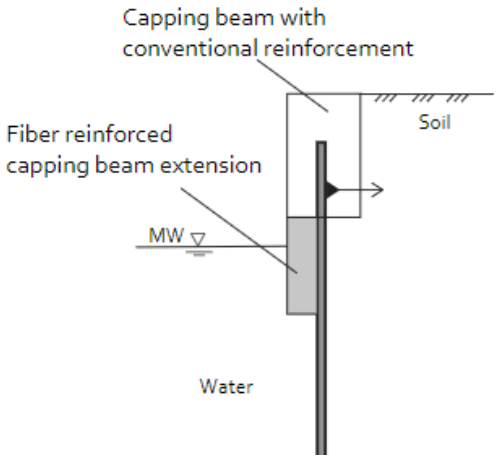

Figure 1.3: *Illustration of the capping beam quay-structure with the proposed design. Fiber reinforced concrete is used for replacing reinforcement bars in the capping beam extension and conventional reinforcement bars are kept in the capping beam.*

1.3 Methodology

In order to verify that the alternative design utilizing fiber reinforcement in the capping beam extension is a possible solution, the crack pattern, crack widths and overall behaviour must be studied. Furthermore, for finding out if the structure has beam behaviour, a numerical model must be used in order to extract results that could be compared with the actual design approaches. In order to achieve the aim of the thesis, the work is divided into two main parts, a literature study and a numerical modelling part, for which a specific project recently carried out by engineers at Ramboll is chosen as a case study.

Initially a literature review emphasized on fiber-reinforced concrete is carried out. Focus is on finding out what reinforcement fiber would be suitable for this type of structure and environment, what design codes are available and appropriate and if fiber reinforced concrete previously has been used for similar projects. The literature study also involves a description of the specific type of structure and how the structure is commonly designed. Corrosion processes are briefly described to get a better understanding of degradation phenomenon.

The literature study is followed by a chapter describing relevant information of the case study that is modelled. FE-analysis is performed in the finite-element software Diana and choices in terms of material models and boundary conditions used etc. are discussed. This particular software is chosen since it offers advanced finite element modelling of reinforced concrete structures with numerous material models implemented, which are needed for analysis of crack patterns.

Firstly, two numerical models are created in Diana, one with conventional reinforcement and one with a fiber-reinforced capping beam extension. The safety of the structure is verified by studying the accurate crack pattern, crack widths and the overall behaviour. Secondly, simple hand-calculations are performed comparing strain values over the support and in mid-span for the FE-model and hand-calculations.

1.4 Limitations

The focus of the thesis is put on one specific case study which limits the scope of the findings which might be influenced by the specific details of the project such as its geometry. For numerical modelling the material models are calibrated in specific tests which might influence the results. Increasing the number of performed tests would yield more accurate results but this has been left out due to time constraints.

In Sweden the current guidelines are providing recommendations for polymer fibers and steel fibers, why these fibers are the only ones to be investigated further in this thesis, even though there might be other fibers suitable for marine environments. For this thesis a few specific load cases will be investigated. In order to completely

verify the safety of the proposed design it would be necessary to investigate all relevant load cases, while some has been left out due to time constraints.

2

Literature Study on Capping Beams, Corrosion and Fiber Reinforcement

2.1 Fiber Reinforced Concrete

Fiber reinforcement consists of small discrete fibres that are mixed into the concrete and could be made out of several different materials, as for example steel, basalt or synthetic materials. The main influence of adding fibers to the concrete is the residual strengths that are obtained after cracking of concrete, since fibers will transfer forces across cracks, yielding an increased ductility in the concrete. By adding fibers into the concrete the durability and mechanical properties can be improved. It may further reduce and prevent development of shrinkage cracks and increase the toughness of the concrete (Zhang et al., 2018). Usually fiber reinforcement is used together with traditional reinforcement and not as a substitute, with the main role to control the cracking process of the concrete. It is generally not used to increase the strength of the concrete, even if some small improvements in strength may arise (Bentur and Mindess, 2006).

2.1.1 Common Applications of Fiber Reinforced Concrete

In Sweden fiber reinforced concrete(FRC) has been used for tunnel linings, since the 1970s, and for industrial floors since the 1980s. For these applications there have been standards and recommendations available (Silfwerbrand, 2020). For load bearing structures, standards has not been provided in Sweden until 2014 (SIS (Swedish Standards Institute), 2018), which has limited its usage in industry.

2.1.2 Similar Projects

For marine applications there are several cases where shotcrete (sprayed concrete) with steel fiber reinforcement successfully has been used for repairing reinforced concrete structures, such as piles, with a method called jacketing (Carl A. Thoresen, 2010). The method basically involves encasing of the damaged structure with a layer of new concrete that could strengthen as well as protect the structure from further deterioration.

One project has been found where fiber reinforcement has been utilized for reinforcing capping beam extensions. The capping beam extension was constructed in Israel and used synthetic fiber reinforcement in order to entirely replace the conventional reinforcement. The capping beam extensions were installed in order to protect an existing quay wall which was already severely damaged from corrosion. The project was successful and it was concluded that this repair alternative could be preferred rather than other common methods, as epoxy coating or steel fiber jacketing, due to its low operational downtime and durability (Chernov and Buslov, 2004).

2.1.3 Design Codes

Even though fiber reinforced concrete has been used frequently since the 1950s for certain applications, usage has generally been quite small due to the lack of standards and recommendations (Silfwerbrand, 2020). However, Sweden, among many other countries, have recently published guidelines for usage in load-bearing structures. The Swedish guideline (SIS (Swedish Standards Institute), 2018) was published in 2014, and is a complement to Eurocode 2. The Swedish guideline is treating steel fibers and polymer fibers, but is in contrast to Eurocode a recommendation, it must not be used in design. According to these recommendations, synthetic fibers are not allowed to be utilized in the ultimate limit state (ULS), while steel fibers must be accompanied by conventional reinforcement if used in marine environments such as the tidal zone, which is the environment of a capping beam.

By adding fibers to the concrete mixture, the behaviour of the concrete changes. After cracking of a fiber reinforced concrete member, it exhibits residual tensile strengths due to the fibers transference of stresses across cracks. The residual flexural tensile strengths are determined from beam testing and typically the fiber reinforced concrete element exhibits a bending softening behaviour, meaning that the flexural strength decreases after cracking and with the increase of strains. The principal stress-strain relationship of fiber-reinforced concrete can be seen in Figure 2.1.

The tensile behaviour of this material is in the Swedish Standard characterized by the concrete tensile strength, and the residual strengths of concrete after cracking due to the fibers. The residual tensile strengths are determined through beam testing according to the Swedish Standard, SS-EN 14651, which is a crack mouth opening displacement test (CMOD). $f_{R,1}$, $f_{R,2}$ and $f_{R,3}$ are corresponding to crack mouth openings of 0.5, 2.5 and 3.5 mm respectively.

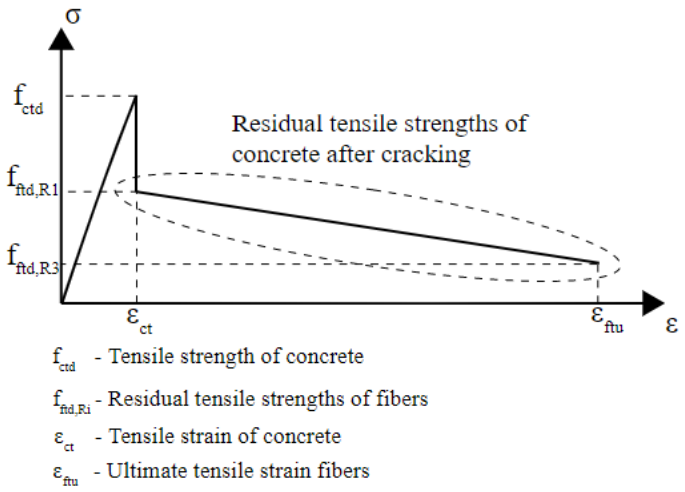

Figure 2.1: *Principal stress-strain relation of FRC in accordance to the Swedish standard SS:812310.*

2.1.4 Different Types of Fibers

Fibres used as fiber reinforcement can be made out of a variety of materials such as steel, natural materials or synthetic materials. Fibers are often classified depending on their geometrical properties such as the aspect ratio, which is the ratio of length to diameter of the fiber, and if its a monofilament or a fibrillated fiber. A monofilament fiber is a large diameter continuous fiber often with a diameter larger than 100 μm and fibrillated fibers are a network of fibers where the individual fiber have branching fibers (Löfgren, 2005). Different fibers and their material properties are summarized in Table 2.1.

Table 2.1: *Mechanical properties of different types of fibers (Löfgren, 2005).*

Material of Fiber	Diameter [μ m]	Tensile Strength [MPa]	Young's Modulus [GPa]
Steel	5-1000	200-2600	195-210
Polypropylene	10-200	310-760	3.5-4.9
Polyvinyl acetate	3-8	800-3600	20-80
Polyethylene	25-1000	80-600	5.0

2.1.4.1 Mechanical Properties

Mechanical performance of FRC depends on many factors including the fibers modulus of elasticity, the length and the aspect ratio of fibers, its bond strength to the concrete matrix as well as the volume of fibers used in the mixture. Generally the concrete exhibits larger residual strengths for an increasing fiber content, but at the same time an increased fiber volume decreases the workability of the concrete (Bentur and Mindess, 2006).

2.1.5 Steel Fibers

Steel fibers can be divided into different groups depending on the manufacturing method, the Swedish standard (Swedish standards Institute, 2006a) categorize groups into cut cold-drawn steel wire, cut sheet fibres, fibres milled from steel blocks, melt extracted fibres and shaved cold drawn wire fibres. These fibres all exists in many geometries and can be either deformed or straight, modern fibres often have a higher slenderness and more complex geometries than traditionally used fibers (Löfgren, 2005).

2.1.5.1 Corrosion of Steel Fibers

The durability of steel fiber reinforced concrete(SFRC) due to corrosion has been investigated by Bentur (Bentur and Mindess, 2006) among many others, with the conclusion that uncracked steel fiber reinforced concrete is highly corrosion resistant. Fibers at the outer surface in SFRC tend to corrode and give unaesthetic stains at the surface. The loss of material at the surface is sometimes dealt with by adding a sacrificial layer of a few millimeters to the cross-section. For cracked concrete, bare fibers within the cracks tend to corrode. These damaging effects can be small if the crack width is kept under a certain critical crack width. Several investigations on the topic shows that the critical crack width for corrosion between cracks is somewhere around 0.1-0.25 mm (Bentur and Mindess, 2006). It has also been shown that reducing the water cement ratio of the concrete can reduce the damage to the fibres. The critical crack width is a controversial topic with disagreements among researchers which can be seen by the large variations in recommended maximum crack widths from different guidelines (Marcos-Meson et al., 2018). It has been seen that in real applications of SFRC in structures the corrosion of steel fibers has been found to be minimal (Tsinker, 1997).

2.1.6 Polymer Fibers

Synthetic polymers are produced by a method called polymerisation, which is a chemical process where a large number of small molecular units are formed into long-chained molecules (Domone, 2018). A numerous of different synthetic fibers can be used in order to reinforce concrete with a wide difference in mechanical properties. As can be seen in Table 2.1 the stiffness of polymer fibers are generally low compared to steel, but there are some synthetic fibers on the market exhibiting both high strength and a high modulus of elasticity. Using fibers with low modulus of elasticity can still yield large improvements with regard to toughness, crack control and strain capacities (Bentur and Mindess, 2006).
According to the Swedish standard (Swedish standards Institute, 2006b) treating polymer fibers, fibers with a length less than 30 mm are called micro fibers (class 1), and fibers above 30 mm are called macro fibers (class 2). If the fibers are used in order to increase flexural strength, class 2 is recommended. Polymer fibers are sensitive to creep and when used, according to the Swedish Standard, the long-term creep properties of the fibers must be evaluated through long-term tests (SIS (Swedish Standards Institute), 2018).

2.1.6.1 Polypropylene (PP) Fibers

Polypropylene fibers are usually manufactured in an extrusion process with circular or rectangular cross-sections. The fibers generally have a low modulus of elasticity and a weak bond with the concrete matrix. There are however polypropylene fibers developed which are referred to as structural fibers. These fibers have an increased elastic modulus, tensile strength and bonding properties compared to ordinary polypropylene fibers. These fibers are often produced by extruding a mixture of both polypropelene and polyethylene fibers (Bentur and Mindess, 2006).

2.1.6.2 Polyvinyl alcohol (PVA) Fibers

The pure form of PVA is a white powder that can be made into fibers to be used in FRC structures. Use of PVA fibers are becoming more common due to its good mechanical properties, none toxicality, high bond strength and its corrosion resistance. Due to its high tensile strength PVA fibers contributes to sustaining the first crack stress and to resisting the pull out force between the fibers and the cement matrix (Noushini et al., 2013). As seen in Table 2.1, PVA fibres typically have a tensile strength of about 800-3600 MPa.

2.2 Corrosion Mechanism

Corrosion starts when a metal is included in a galvanic cell consisting of an anode, cathode and an electrolyte, such as water. At the anode, the negative pole, oxidation of ferrous ions takes place whilst at the cathode the reduction reaction is taking place. Furthermore an electrolyte in the form of water containing free ions acts as an electric conductor (Tsinker, 1995). The oxidation and reduction process happens simultaneously and can be described by Equation 2.1.

$$\begin{aligned} H_2O + O2 + 4e^- &\rightarrow 4OH^- \\ Fe &\rightarrow Fe^2 + 2e^- \end{aligned} \tag{2.1}$$

2.2.1 Corrosion of Steel in Concrete

Steel embedded in concrete is often already corroded on the steel surface, and the oxidation product of a very thin film layer of ferric oxide, Fe_2O_3, is covering the surface. This thin layer is very stable and referred to as passive film. The passive film protects the metal from further corrosion when embedded in high alkaline cement and can be broken either by the effect of PH-value of the concrete closest to the reinforcement is lowered due to carbonation of concrete, or by intrusion of chlorides from the sea water reaching a critical chloride level within the concrete (Tsinker, 1995). The effect of corrosion is rust that is formed near the reinforcement, rust takes up several times more volume than steel resulting in spalling and cracking of concrete. Spalling and cracking will increase the corrosion rate further by exposing the steel to more oxygen and chlorides (Carl A. Thoresen, 2010).

For marine environments the relative humidity is very high, creating an aggressive environment for metals directly exposed to the surroundings. Corrosion of exposed steel is a common problem in marine structures and the chlorides in the seawater is the major contribution to initiation of steel corrosion (Alexander, 2016). Waterline corrosion takes place because of differences in oxygen concentrations around the surface water level. Steel areas exposed to higher oxygen levels becomes the cathode, and the area exposed to less oxygen will act as the anode (steel area under water). Approaches to protect the steel from corrosion can be made by either adding a protective layer of coating on to the metal or by installing a substructure covering the steel completely thus protecting it from oxygen and chloride attacks. It has also been proven that inducing an electrical current can change the environment around metal and work to decrease the corrosion rate (Domone, 2018, p.106).

2.2.2 Corrosion Rates in Sheet Piles

Sheet pile walls are according to the Swedish Standard on piles and sheet piles categorized into zones depending on the aggression of the environment, which determines the corrosion rate to which the structure is subjected. The most aggressive zones in sea water are the splash zone and the lower water zone, A and C respectively, see Figure 2.2, due to the cyclic periods of sea water constantly wetting and drying the structure. The zone between the mean high water, MHW, and mean low water, MLW, is called the intertidal zone (zone C) and for most cases it phases less risk of corrosion than the splash and lower water zones. Parts of a structure below the sea level is referred to as a submerged zone, zone D, that has less risk of corrosion damage to steel due to the lack of oxygen. The lowest rate of corrosion is observed in the buried zone, zone E (SIS (Swedish Standards Institute), 2007).

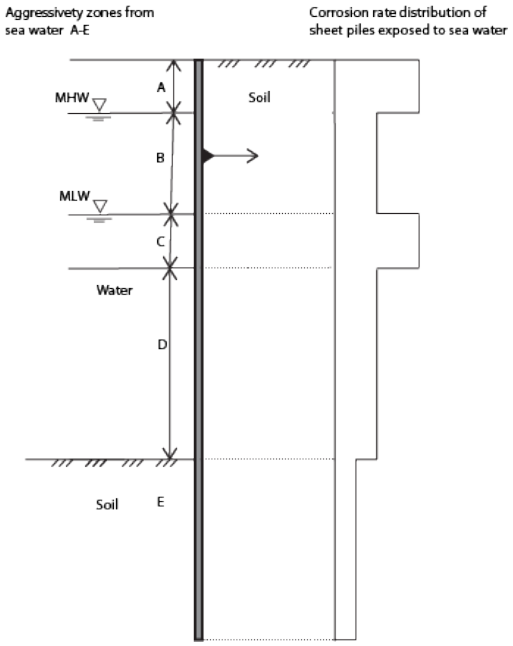

Figure 2.2: *Sea water zones divided into different aggressivity zones, zones A-E. (SIS (Swedish Standards Institute), 2007).*

Loss of material thickness of sheet piles due to corrosion has to be considered in the design, the Swedish Standard on steel structures of piles provides corrosion rates as millimeters of material loss per year, some examples of values relevant for a quay wall can be seen in Table 2.2 for sea water exposure and Table 2.3 for soil exposure. For sheet piles in contact with water on one side and soil on the other, corrosion rates apply to each side (SIS (Swedish Standards Institute), 2007).

Table 2.2: *Examples of rates for loss of material in sheet pile walls due to corrosion from sea water, in millimeters, (SIS (Swedish Standards Institute), 2007).*

Sea water temperate climate	25 years	50 years	100 years
Low water or splash zone [mm]	1.90	3.75	7.5
Permanently immersed or intertidal zone [mm]	0.90	1.75	3.5

Table 2.3: *Examples of loss of material in sheet pile walls due corrosion from soils, in millimeters, (SIS (Swedish Standards Institute), 2007).*

Soil type	25 years	50 years	100 years
Undisturbed natural soils [mm]	0.30	0.60	1.20
Non-compacted and aggressive fills [mm]	2.00	3.25	5.75

2.2.3 Concrete Exposure Classes

For concrete structures different environments results in different aggressiveness with regards to deterioration off the structure. According to SIS, this is considered by dividing the different environments into a number of exposure classes. For each exposure class there are specific requirements with regard to crack widths, cover thicknesses, concrete quality etc. Exposure to chlorides from sea water is found in exposure classes XS, described in Figure 2.4 (SIS (Swedish Standards Institute), 2005).

Table 2.4: *Description of exposure class XS - corrosion caused by chlorides in sea water (SIS (Swedish Standards Institute), 2005).*

Exposure Class	Description of Zone
XS1	Exposed to airborne salt, not in direct contact with sea water
XS2	Permanently submerged
XS3	Cyclic wet and dry. Splash zone, tidal zone.

2.3 The Capping Beam Structure

2.3.1 Capping Beams

Capping beams are used to cover and connect piles forming a retaining wall and is often made out of reinforced concrete. The capping beam mainly distributes forces acting on the top of the retaining wall onto the pile row. Capping beams are not only used for quay structures, but also for foundation pits and buildings, both as permanently and temporary constructions (Wells, 2010). For usage in quay structures the concrete cap, besides acting as a stiff top of the retaining wall, can also be extended such that it protects the retaining wall from seawater and corrosion in the tidal zone. Using a concrete cap is often an economical and reliable way of achieving the service life of quay structures, compared to methods such as coatings or sacrifical anodes, the latter also works poorly in the tidal zones (Alexander, 2016). The structure analyzed in this thesis is a quay wall constructed of sheet piles with one anchoring level and a concrete cap along the pile tips. For this structure the wall capping is usually designed to be sufficiently wide for installation of bollards and support rails on its top, and fenders along its height (Carl A. Thoresen, 2010).

2.3.2 Design

A capping beam used in a quay structure must be designed to carry both horizontal and vertical loads. In this thesis the load carrying abilities in the horizontal direction are investigated. The design of the capping beam in the horizontal direction could be based on the calculations from the sheet pile wall design. In these calculations the force in the anchors is calculated. Knowing this force, it could be assumed that it is evenly distributed onto the capping beam. The capping beam could then be assumed to be acting as a continuous beam supported by the anchors, as illustrated in Figure 2.3.

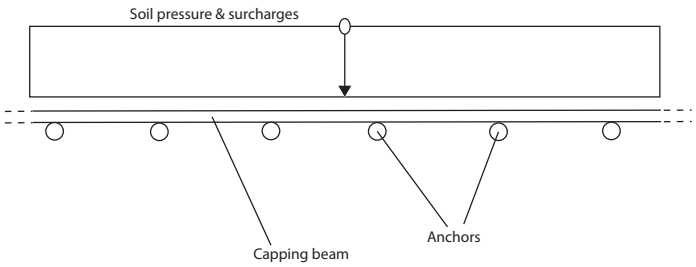

Figure 2.3: *Plan view of capping beam idealized as a continuous beam supported by anchors.*

As the capping beam is a part of a retaining wall, it must be designed to be able to carry earth pressures acting on the wall as well as geotechnical loads such as surcharges. Furthermore, the capping beam must be designed to carry bollard actions from berthed vessels and impact forces from vessels hitting fenders. As bollards and fenders are placed with a certain spacing and since fender and bollard actions often impose large stresses on the capping beam, such sections could be added with extra reinforcement as well as additional anchors, thus reducing the span width at these sections.
Furthermore, in design of capping beams one load case that is often considered is the loss of an anchor, corresponding to an accidental load case, according to practicing engineers at Ramboll. By the loss of an anchor the span length of the capping beam is doubled, while loaded by earth pressures in rest and possibly an additional surcharge acting behind the retaining wall.

In design of capping beams the connection between the capping beam and the sheet pile wall is commonly secured by passing reinforcement through the sheet piles. Also, concrete is cast with a waling beam inside which will act as a shear connector. For the capping beam extension the connection is usually secured by welding of vertical reinforcing bars onto the sheet piles(Broeken, 2014), that will act as shear connectors.

2.3.3 Interaction Steel and Concrete

Capping beams are composite structures composed of concrete beams and steel sheet piles. To be able to transfer shear load at the interface between two elements it is often required to use some kind of mechanical shear connector of various shape (Bradford and A., 1995). For capping beam extensions, reinforcement bars are often used as shear connectors as they are welded directly onto the sheet piles in order to bond the materials together (Broeken, 2014). If the capping beam extension is cast with most of the conventional reinforcement replaced by fiber reinforcement, it is necessary to investigate if the shear connectors are needed or if shear stresses between the elements are so small that adhesion is sufficient.

Composite interaction between steel and concrete without the use of any shear transfer attachment can be described by chemical adhesion and friction that transfer shear forces by bond between the materials. In case of interface slip between the concrete and steel the chemical adhesion is lost (Bradford and A., 1995). If not using any shear connectors it must be known how large shear stresses can be before the adhesion between materials is lost. By experiments found it has been seen that the adhesive strength between steel sheets and concrete for an untreated surface is at least 0.75 MPa, the experiments were performed on non corroded steel plates (Berthet et al., 2011). Worth noticing is that the influence of rust on the steel surface is beneficial for the steel-concrete bond strength (Degée et al., 2017).

3

Methodology & Case Study

In this chapter the reference project for the case study is introduced along with relevant project specific information. The setup of the numerical model is described along with material models used as well as performed material validations.

3.1 Reference Project

The chosen reference project for this thesis is a capping beam designed by Ramboll as a part of a new ferry location. A picture of the case study during production can be seen in Figure 3.1, where all sheet piles have been installed.

Figure 3.1: *Picture taken during construction of the project for the case study (*PEAB*, 2021).*

In Figure 3.2 the installed sheet piles can be seen and the production of the capping beam has been started. In Figure 3.3 the installed sheet piles with a waling beam and anchors attached on the land side are displayed, as well as some parts of the capping beam.

Figure 3.2: *Installed sheet piles, the production of the capping beam has started (*PEAB*, 2021).*

Figure 3.3: *Installed sheet piles, before installation of the capping beam (*PEAB*, 2021).*

3.1.1 Geometry

A section of the capping beam and the capping beam extension including an anchor, reinforcement and the waling beam is shown in Figure 3.4.

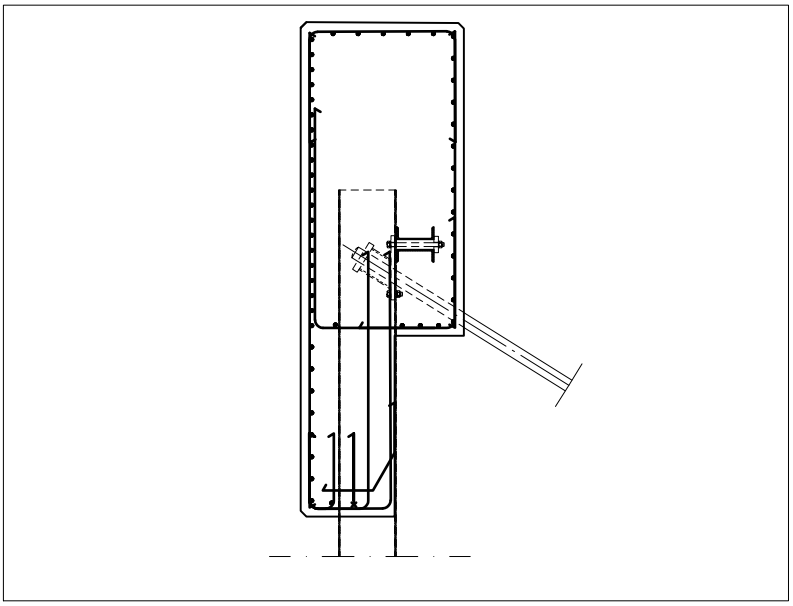

Figure 3.4: *Section of the capping beam and the capping beam extension including an anchor and reinforcement (Ramboll, published with approval).*

3.1.2 Materials

3.1.2.1 Concrete and Reinforcement

The concrete used for the capping beam is of class C35/45. Based on the specific exposure class the characteristic crack widths shall be limited to 0.2 mm. Characteristic strength values of this concrete are summarized in Table 3.1.

Table 3.1: *Properties of the concrete used in the project.*

Concrete	Notation	Char. value
Young's modulus	E_{cm}	34 GPa
Mean tensile strength	f_{ctm}	3.2 MPa
Mean compressive strength	f_{cm}	43 MPa

Reinforcement has a yield strength of 500 MPa and an elastic modulus of 210 GPa. Partial factors according to Eurocode are used in design. Besides taking partial

factors into account, the stiffness of concrete is reduced due to taking creep into account in all load cases. The adopted creep factor is 1.5. All factored material properties used for the serviceability limit state(SLS) and ultimate limit state(ULS) load cases are summarized in Table 3.2. For the accidental load case(ALS), SLS values are used.

Table 3.2: Properties of the concrete and reinforcement used in the project.

Concrete	Notation	SLS	ULS
Young's modulus	E_{cd}	13.6 GPa	28.3 GPa
Mean tensile strength	f_{ctd}	3.2 MPa	2.13 MPa
Mean compressive strength	f_{cd}	43 MPa	
Reinforcement			
Young's modulus	E_s	210 GPa	
Yield stress	f_y	500 MPa	435 MPa

3.1.2.2 Fiber Reinforced Concrete

Relevant technical properties of the chosen fiber are found in Table 3.3, where characteristic strength values are stated along with factored values for ALS and ULS. The technical properties belong to a polymer fiber and its residual tensile strengths are relatively low. If necessary these could be enhanced by changing fiber or increasing the fiber content. For clarification of residual strength values, see the provided stress-strain curve in Figure 2.1. It has been decided to limit the characteristic crack widths of the FRC to 0.2 mm, similarly as for the conventionally reinforced concrete.

Table 3.3: *Properties of the proposed fiber for the capping beam extension.*

Fiber	Characteristic	ALS	ULS
Residual Tensile Strength, $f_{ftd,1}$	1.5 MPa	0.68 MPa	0.63 MPa
Residual Tensile Strength, $f_{ftd,3}$	1.0 MPa	0.43 MPa	0.40 MPa
Length	60 mm		

3.2 Finite Element Modelling

3.2.1 Concrete Modelling

There are three approaches for modelling cracking of concrete; discrete, smeared and embedded crack approaches. For this project a smeared crack approach is used since this does not require special elements to model the cracks, nor does the location of cracks need to be known beforehand, making the method convenient during modelling if all crack information is not known (Plos, 2000). The fracture energy along with the tensile strength of concrete and the stress-crack opening relation is needed in order to model the cracking process. The fracture energy is defined as the area under the stress-crack opening curve. This area represents the total energy that is consumed during the fracture process when completely breaking the material. The

fracture energy (G_f) is related to the mean compressive concrete strength (f_{cm}), as shown in Equation 3.1, (CEB, 2010), where the fracture energy of the used concrete is calculated.

$$\begin{aligned} G_f &= 73 \cdot f_{cm}^{0.18} = 144 N/m \\ f_{cm} &= 43 MPa \end{aligned} \tag{3.1}$$

Two different material models for the behaviour of concrete have been used in modelling. The total-strain based and the multi-directional fixed crack model. The tensile behaviour of conventionally reinforced concrete is assumed to follow a non-linear softening curve as proposed by Hordijk (DIANA FEA, 2021).

3.2.2 Modelling of Fiber Reinforced Concrete

Fiber reinforced concrete is similar to conventional concrete modelled by using total-strain based and multi-directional fixed crack models, but with different settings for the non-linear softening curves after cracking due to the residual tensile strengths arising from the addition of fibers. The adopted stress-strain tensile behaviour of fiber concrete is illustrated in Figure 3.5.

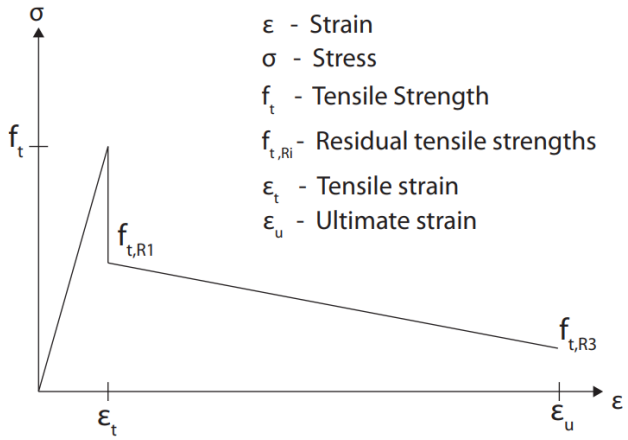

Figure 3.5: *Adopted stress-strain tensile curve for fiber reinforce concrete.*

3.2.3 Modelling of Conventional Reinforcement and Bond-Slip

Reinforcement is modelled using the CEB/FIP Model Code 2010 which provides a relation between the bond stress related to the reinforcement slip (CEB, 2010). A bond-slip relation is used since the actual crack pattern and crack widths in the structure are of interest. The schematic relation between reinforcement bond stress and slip is shown in Figure 3.6. The reinforcement is assumed to follow the Von Mises plasticity behaviour without hardening, as a conservative assumption.

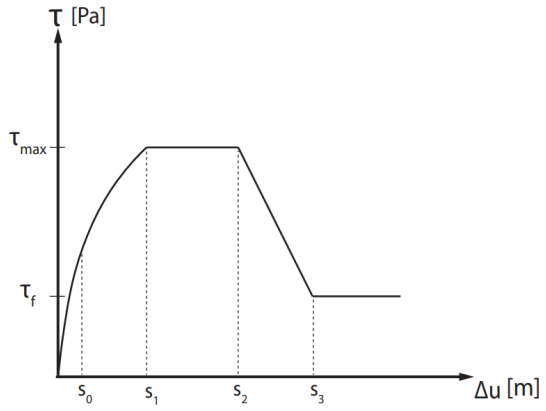

Figure 3.6: *Schematic relation between bond stress and reinforcement slip according to the CEB/FIP Model Code 2010, with notation corresponding to input in Diana.*

3.3 Material Models Calibration

In order to validate the different material choices and therefore to assure that the model will yield trustworthy results, materials are calibrated in simple test setups to obtain the needed material models and its parameters. Concrete and reinforcement properties are calibrated in a tension stiffening test of a thin prismatic specimen and the results are calibrated to match analytical formulations provided in Eurocode. The fiber reinforced concrete properties are tested in a tensile dog bone test modelled in Diana, and the model is calibrated to experimental tests performed by B. Akcay (Akcay, 2012).

3.3.1 Tension Stiffening Test of Reinforced Concrete

In order to study the cracking process of the concrete a thin prismatic concrete specimen reinforced with one bar, is loaded in tension until several cracks appear. The tested beam has a cross-section side of 120 mm and a reinforcement bar with a diameter of 20 mm, resulting in a reinforcement amount of 2.2 %. The geometry of the simulated test specimen is shown in Figure 3.7.

Figure 3.7: *Geometry of prismatic member simulated in the tension stiffening test.*

The concrete crack material models tested are the total strain based and multi-directional fixed crack model. The input parameters for the bond-slip relation are obtained through the CEB/FIB Model Code (CEB, 2010). The parameters are then calibrated in order to obtain the crack pattern and crack widths to be correlated with Eurocode, as accurately as possible. The used input parameters for the bond-slip model are stated in Table 3.4. In Figure 3.8 the created model is shown with crack width output displayed as an example.

The results from modelling is compared with analytical formulations for calculation of crack widths and crack spacing, in Eurocode (SIS (Swedish Standards Institute), 2005). Both maximum and mean values are compared. All hand calculations can be seen in Appendix A. Results are summarized in Table 3.5. From the results it can be seen that both models are yielding results close to the analytical formulations. Due to difficulties with convergence while using the multi-directional fixed crack model, the total strain based model will be used for the reinforced concrete in the FE-model.

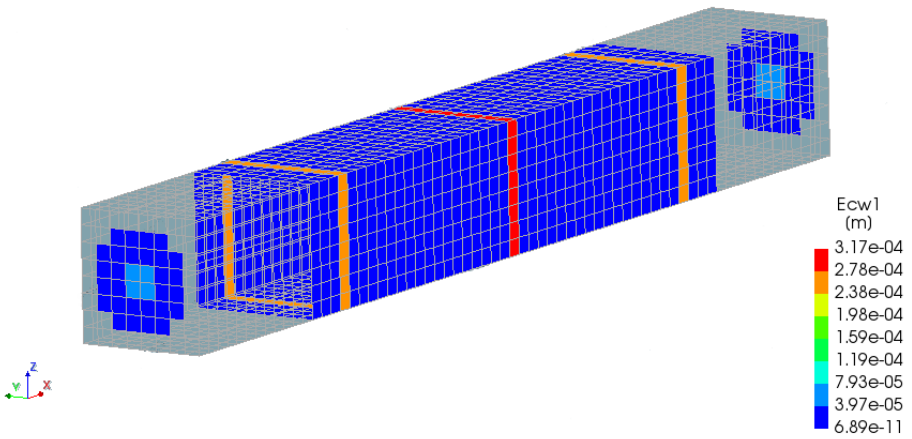

Figure 3.8: *Tension stiffening test in Diana total strain based, crack width output is displayed.*

Table 3.4: *Input parameters for bond-slip model.*

CEB/FIP Parameter	Description	Value
τ_{max}	Maximum bond stress	17 MPa
τ_f	Ultimate bond stress	6.6 MPa
s_0	Initial linearized section	0.025 mm
s_1	Slip parameter, see Figure 3.6	1 mm
s_2	Slip parameter, see Figure 3.6	2 mm
s_3	Slip parameter, see Figure 3.6	8 mm

Table 3.5: *Comparison of results for the FEM-model and Eurocode calculations. Crack widths are calculated at the steel stress of $\sigma_s = 250MPa$, for all calculations. Crack spacing and crack widths in millimeters. S_r is the notation for crack spacing and w_k is the notation for the crack width.*

Diana	S_r [mm]		$w_k(\sigma_s)$ [mm]	
Total Strain Based	267		0.317	
Multi-Dir. Fixed Crack	270		0.295	
EuroCode	$S_{r,max}$ [mm]	$S_{r,mean}$ [mm]	$w_k(\sigma_s)$ [mm]	$w_{k,mean}(\sigma_s)$ [mm]
	452	266	0.340	0.200

3.3.1.1 Tension Stiffening Test - Mesh Sensitivity

In order to evaluate the models sensitivity to mesh refinements three different mesh sizes are tested and the results are compared. The results obtained from mesh changes are summarized in Table 3.6. From the test it is concluded that the analysis is mesh independent.

Table 3.6: *Results from mesh sensitivity test. S_r is the notation for crack spacing and w_k is the notation for the crack width.*

Mesh element length	S_r[mm]	$w_k(\sigma_s)$ $[mm]$
12 mm	265	0.255
15 mm	259	0.250
30 mm	272	0.262

3.3.2 Tensile Test of FRC

A comparison between a lab test from literature of FRC specimens and a model with the same geometry and material parameters in Diana is conducted. From study on the tensile behaviour of FRC by B. Akcay (Akcay, 2012) has been selected to verify the material model of FRC to be used in Diana. The study examines tensile behaviour of FRC as well as the influence of fiber content in concrete mixture. Geometry of the concrete block investigated and the attached pendulum-bar system setup for measurement is shown in Figure 3.9.

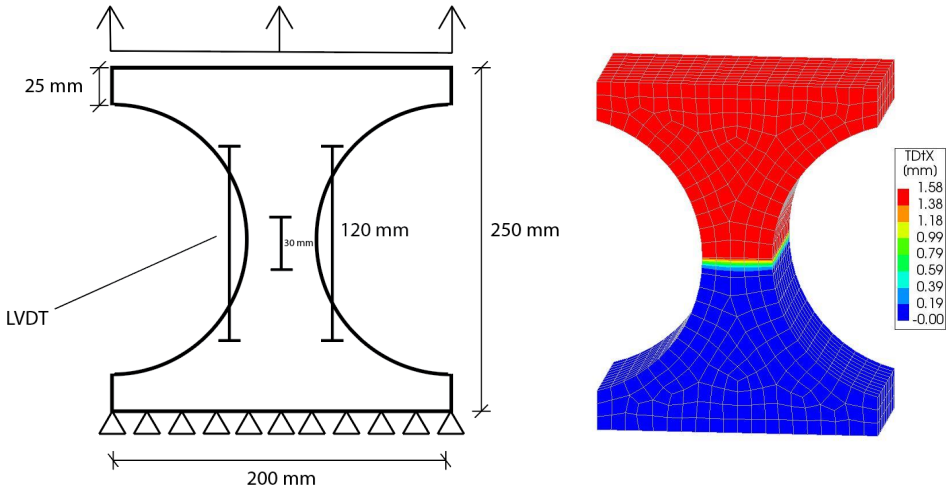

Figure 3.9: *Tensile test geometry and boundary conditions. Left figure shows the placement of LVDT meters, boundary conditions and load application, right figure shows the displacement of the specimen in the direction of the force applied.*

On the specimen four LVDT's (linear variable displacement transducers) are attached to measure the displacement and strain of the specimen. Material parameters used for the tensile test in Diana calibrated from the studied lab test can be found in Appendix B.

Sets of data from the tensile test for the load displacement curve as well as the stress-strain behaviour have been compared to results from the numerical simulation in Figure 3.10. The load displacement curve of the two material models corresponds well with the average load displacement from the lab test.

It can be concluded that the behaviour of both the multi-directional fixed crack model and the total strain based model are showing similar behaviour of that of the lab test. The difference between the material models are small but it may be stated that the multi-directional material model follows the behaviour of the lab test better, and so it may be preferable for further modelling.

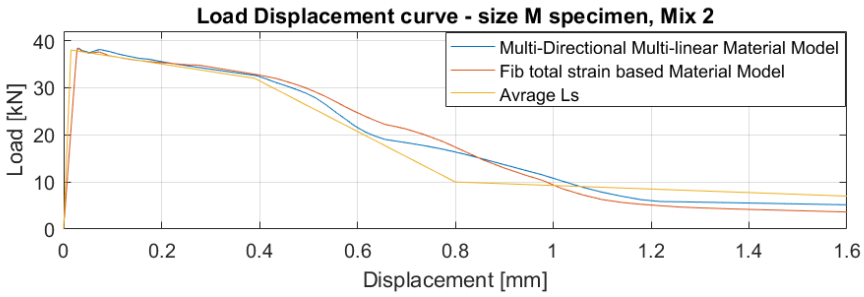

Figure 3.10: *Load - Displacement curve of test results and simulation. Yellow line Ls is the tensile test lab data.*

3.4 FEM-model of the Capping Beam Structure

The created FEM-model is based on the geometry of the structure used in the case study, presented in Chapter 3. Three different load cases are analysed, one load case in the serviceability limit state, one in the ultimate limit state and one in the accidental limit state. In order to ensure that the analyses are yielding correct results, it is needed to calibrate and verify that the models are working correctly. In order to do that, the geotechnical analysis performed by Ramboll in the design of the sheet pile wall for the case study has been used as a reference. Plots from the geotechincal analyses can be found in Appendix C & D. The procedure of the calibration is described in the coming sections. For the project a vertical coordinate system starting at 3.09m at the top of the capping beam has been used, this coordinate system will be referred to during coming sections. See Figure 3.11 for reference heights of the structure. The studied load cases with short descriptions can be seen in Table 3.7.

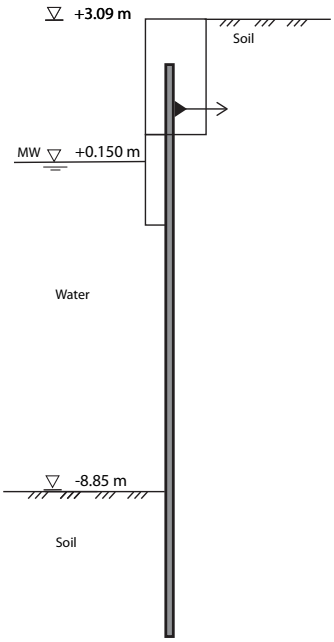

Figure 3.11: *The quay structure along with the used vertical coordinates in the project. Sketch is not true to scale.*

Table 3.7: *Studied load cases SLS, ALS & ULS with short descriptions.*

Load case	Description
SLS	Net pressure from soil in rest
ULS	Net pressure from soil in failure + surcharge
ALS	Failure of an anchor under SLS loading conditions

3.4.1 Geometry and Boundary Conditions

Anchors are located with a spacing of 4.2 meters. In order to decrease the influence of the boundaries in the modelled geometry five spans are modelled, resulting in a modelled length of 21 meters. In order to decrease the modelled height and its complexity the entire sheet pile wall is not modelled, but the modelled geometry is kept large enough such that deformations in the sheet piles can be visualized and verified against the geotechnical model. The sheet piles are supported at its bottom sections and prevented to move vertically (z-direction) and to translate towards the sea (y-direction).
In the serviceability limit state the sheet piles are ending in the zero moment section, why the sheet piles are allowed to rotate freely around this point. However, as the zero moment section varies for different load cases while the modelled height is kept constant, for the ULS case, a bending moment has been applied to the sheet pile flanges instead. At the right and left boundary of the modelled geometry, the sheet pile and the concrete beams are supported such that translations in the x-direction are prevented. The entire modelled geometry can be seen in Figure 3.12, while the modelled concrete, the capping beam and its extension, can be seen in Figure 3.13.

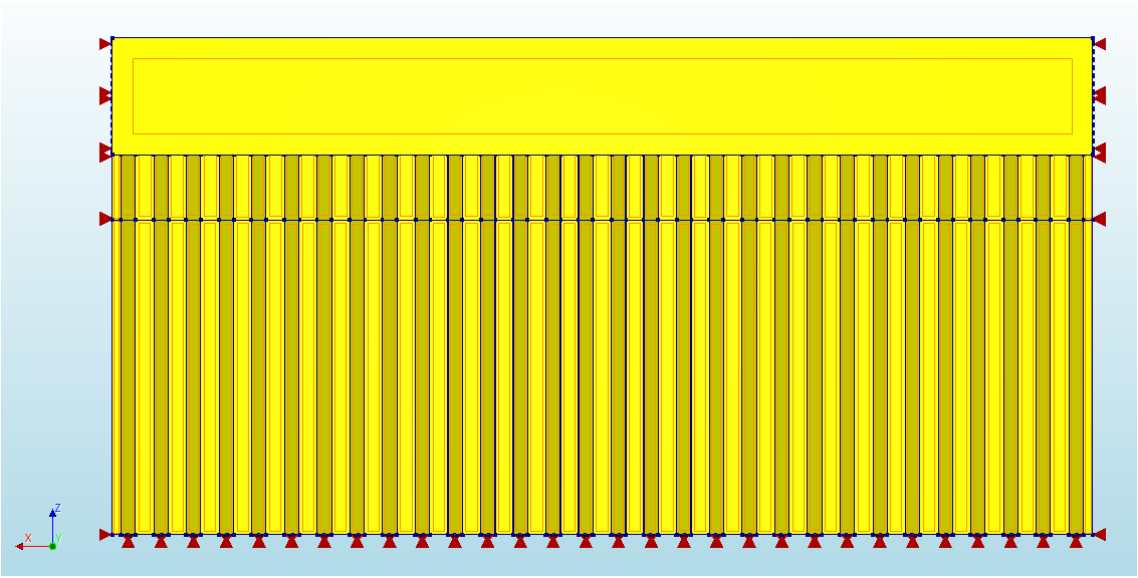

Figure 3.12: *Sheet pile wall and capping beam structure viewed from land side, with boundary conditions on the sheet piles displayed. Load application from soil pressure shown as orange lines applied in plane.*

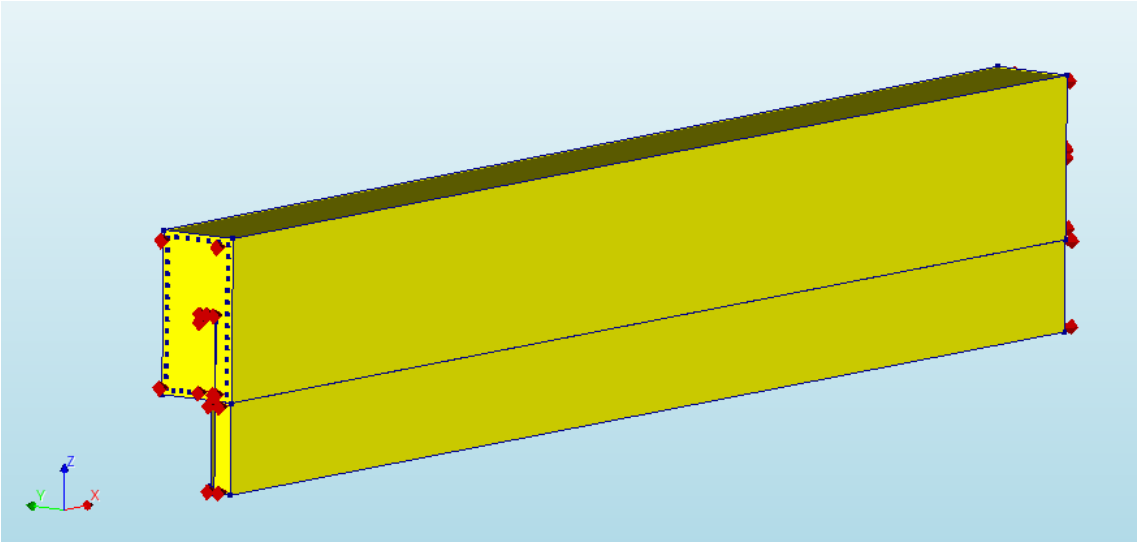

Figure 3.13: *The geometry of the capping beam and the capping beam extension. View from sea side.*

The tie-back anchors are not modelled in Diana. Instead boundary conditions as shown in Figure 3.14 are introduced. The figure is showing supports at the location of the anchors, with the same size as the plates that support the anchors. The supports are introduced between the concrete and the sheet piles. These supports are for one model given prescribed deformations, while for another spring stiffness supports are introduced. These two models will be described more into detail in the coming section. At the bottom of the sheet piles, there are displacements of the wall towards the sea side. At this level prescribed deformations are applied according to the geotechnical analyses, Appendix C & D.

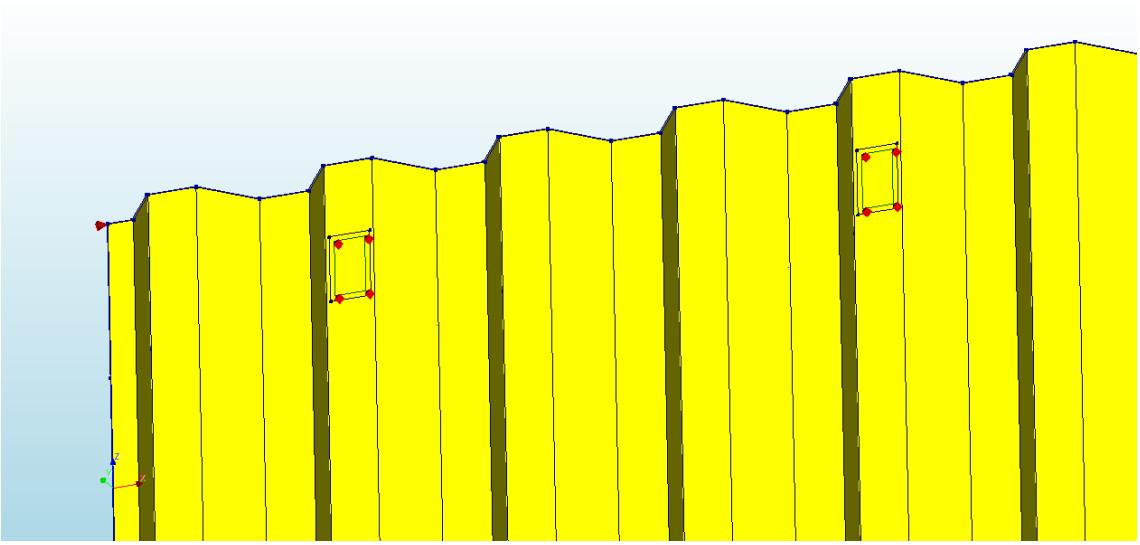

Figure 3.14: *Anchor plates on sheet piles viewed from sea side. Anchor plates are modelled as supports.*

All modelled reinforcement can be seen in Figure 3.15 with the conventionally reinforced alternative in the top, and the fiber reinforced alternative in the bottom of the figure. Sections of the alternatives are shown in Figure 3.16. As shown in the figures, in the model with fiber reinforced concrete all longitudinal bars and some stirrups are removed from the capping beam extension. The kept stirrups are shortened and extended into half the height of the extension, in order to provide a strong connection between the capping beam and its extension. Reinforcement bars are embedded into concrete, see section 3.2.3 for modelling choices.

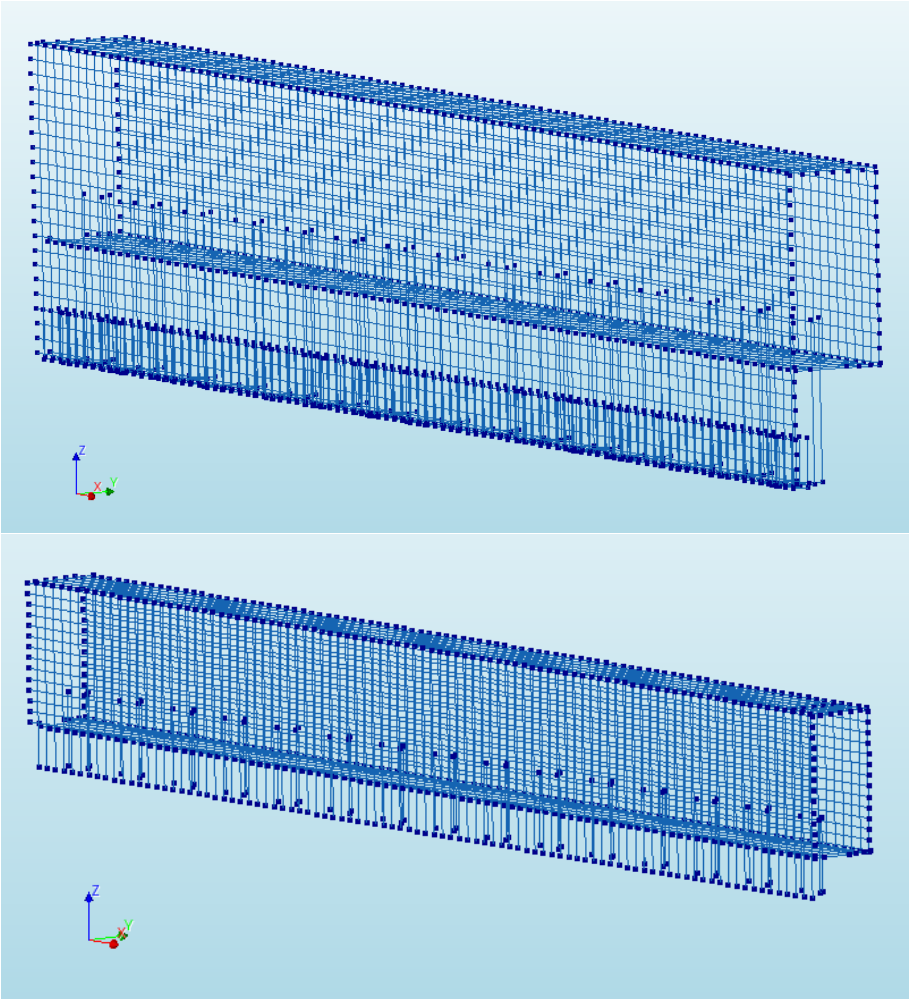

Figure 3.15: *Modelled stirrups and longitudinal bars of the structure for conventionally reinforced concrete (top) and fiber reinforced concrete (bottom). Model with fiber reinforcement has less reinforcement bars in the capping beam extension.*

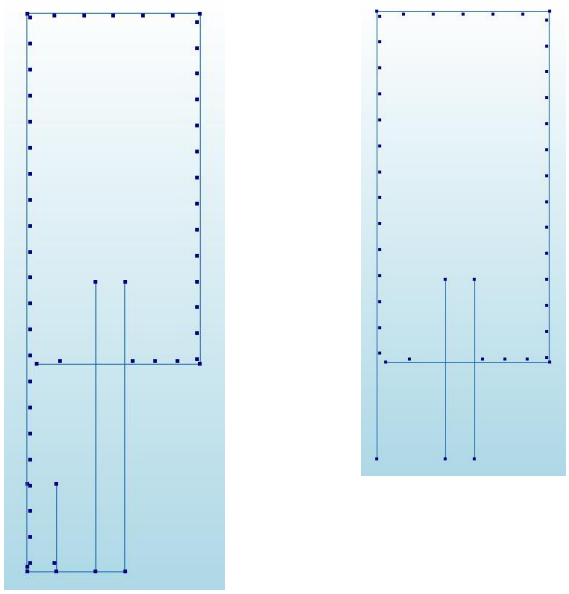

Figure 3.16: *Sections of reinforcement arrangements. Conventionally reinforced according to the case study (left) and the proposed design with a fiber reinforced capping beam extension (right).*

The used mesh for all load cases can be seen in Figure 3.17. The elements are quadratic with a mesh size of 250 mm, this was chosen due to mesh size independence when using embedded reinforcement, as shown in Chapter 3.3.

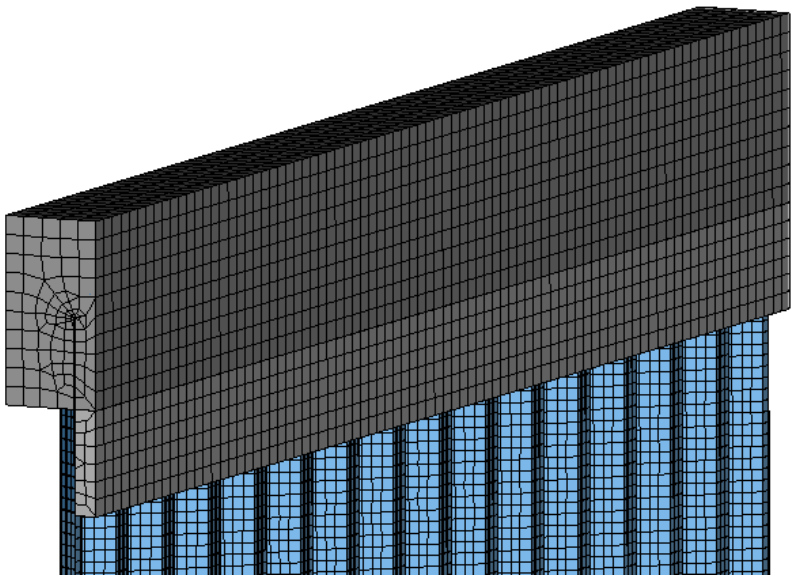

Figure 3.17: *Mesh size of model, figure shows an element mesh size of 250 mm which has been used in the SLS, ALS & ULS model.*

3.4.2 Simplifications

Several simplifications were made in order to reduce the complexity of the model, as described in this section.

- Soil is not modelled in Diana, instead pressures obtained from geotechnical analyses have been used.
- Since the concrete parts are what is investigated in this thesis, it is assumed that the sheet piles remains in the elastic range.
- For the numerical modelling full interaction between the sheet piles and the reinforced concrete is assumed for all models.
- The anchors are not modelled, instead supports are added inside the concrete at the location of the plates where anchors are attached. These supports are given a spring stiffness or a prescribed deformation such that they are allowed to translate. In reality there are anchors of about 20 meters length running from the sheet pile into the ground.
- Anchors are assumed to be completely horizontal and perpendicular to the concrete beam, whilst in the actual structure anchors are inclined, as seen in Figure 3.4.
- For the calibration a spring stiffness was verified for the case without a capping beam. This spring stiffness is then assumed to be unchanged for the structure including the capping beam.
- In the vertical direction rigid supports are used at the bottom of sheet piles, in order to make modelling simpler. In reality the soil is not rigid and sheet piles may be displaced vertically.
- The waling beam is completely removed when modelling the structure with the concrete capping beam. Keeping the waling beam would increase the stiffness of the system.

3.4.3 Loading - SLS & ULS

The loading for the SLS and ULS load cases are plotted in Figure 3.18. The loading differs from the stages as the SLS case is considering characteristic soil values in rest while soil is assumed to fail in ULS and partial factors are used. Furthermore, the ULS load includes surcharges acting behind the quay wall. The conditions at site for the chosen stages are illustrated in Figure 3.19. This figure shows that the wall has been back-filled with soil up to the coordinate of 3.09 meters. It also shows that the flexural stiffness of the wall is reduced, for both load cases, to two different values due to corrosion of the wall.

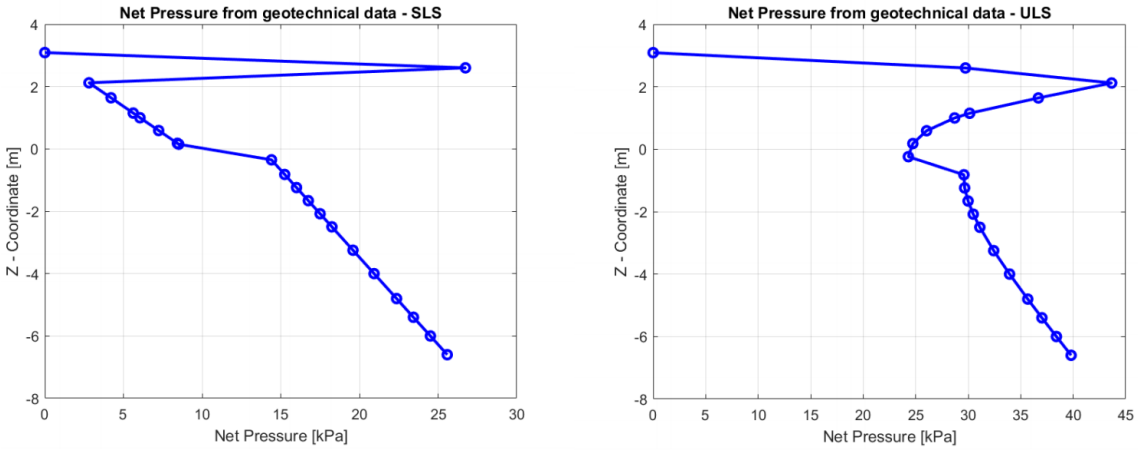

Figure 3.18: *Net pressures for SLS & ULS, obtained values from the geotechnical analysis.*

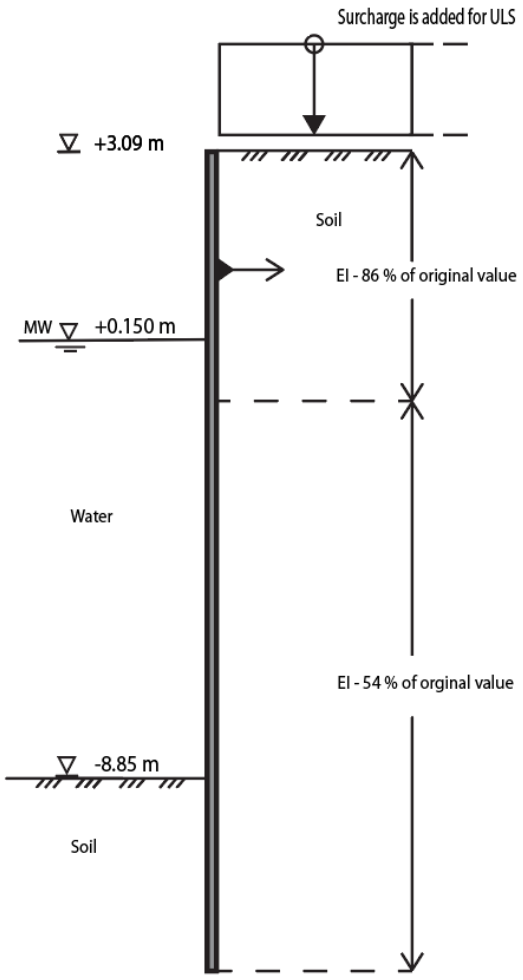

Figure 3.19: *Loaded structure by soil and surcharge. Corrosion causes the flexural stiffness of sheet piles to change due to loss of material.*

The applied loads are on the conservative side since in reality the sheet piles are installed and soil is placed to a level of about +1.0 meter, after that the capping beam is cast and afterwards the rest of the soil is placed. Thus, the sheet pile is already loaded with some of the net pressures and allowed to deform before concrete is cast and the final soil is placed, while in the created FE-model, all net pressures are assumed to act on the structure with the capping beam.

As the modelled height is smaller than the actual height of the sheet piles, different boundary conditions must be used for the SLS case and the ULS case. The SLS model is modelled to the coordinate of the zero moment section, why the sheet pile is allowed to rotate around its end section. For the ULS model, there is a bending moment in the sheet pile at the end section, which has been applied to the flanges as a force couple.
For both the ULS and SLS models, the end section of the sheet piles are given horizontal displacements according to geotechnical analysis.

3.4.4 Calibration of Model

Two different modelling approaches have been implemented. One utilizing a linear interface stiffness at the position of the tie-back anchors and another one with prescribed deformations at the same positions. The overall displacements are similar through both modelling approaches, but the main difference is that the model with prescribed deformation is more rigid and less prone to rotate around its anchor position.

3.4.4.1 Calibration of Model - Spring Interface

The calibration process and verification of the model is based on the previously mentioned analysis performed by geotechnical engineers that designed the sheet pile wall for the case study. Calibration of models has involved applying the same loading conditions as in the geotechnical analysis, while the spring stiffness of the anchors has been changed until the results from Diana are matching the results from the geotechnical analysis. This calibration procedure has been repeated for two different stages of the geotechnical calculations which have been chosen to represent the earlier described ULS & SLS loading scenarios.

The sheet pile displacements with the calibrated stiffnesses are shown in Figure 3.20 along with the corresponding geotechnical data used for calibration. In this geotechnical analysis the capping beam was not included. The adopted spring stiffness is assumed to be linear and the calculated stiffness of the spring is assumed to be unchanged after the capping beam is cast.

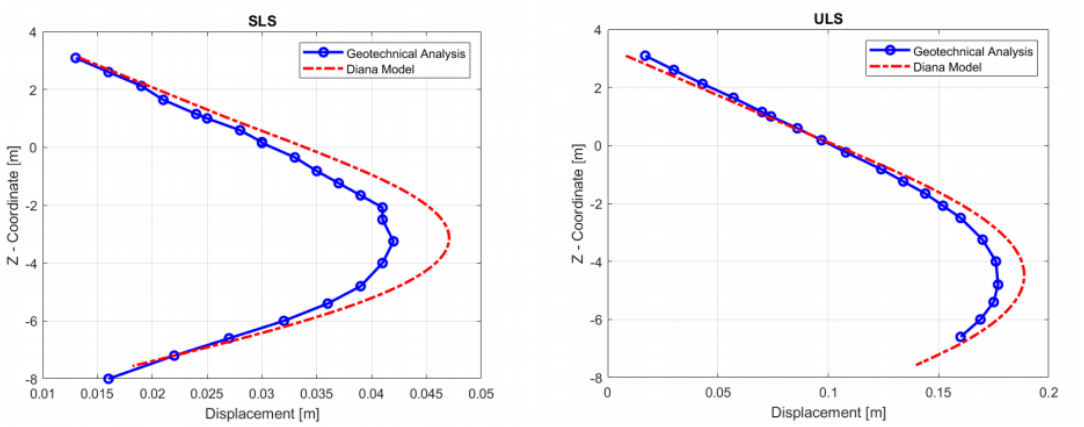

Figure 3.20: *Displacements of the sheet pile walls under SLS and ULS loading, Diana model and results from geotechnical analysis.*

3.4.4.2 Calibration of Model - Prescribed Deformation

For the model with prescribed deformations on the anchor plates, displacements according to the geotechnical analyses are prescribed both to the anchor positions as well as the end sections, in order to verify the structural behaviour. The results are shown in Figure 3.21.

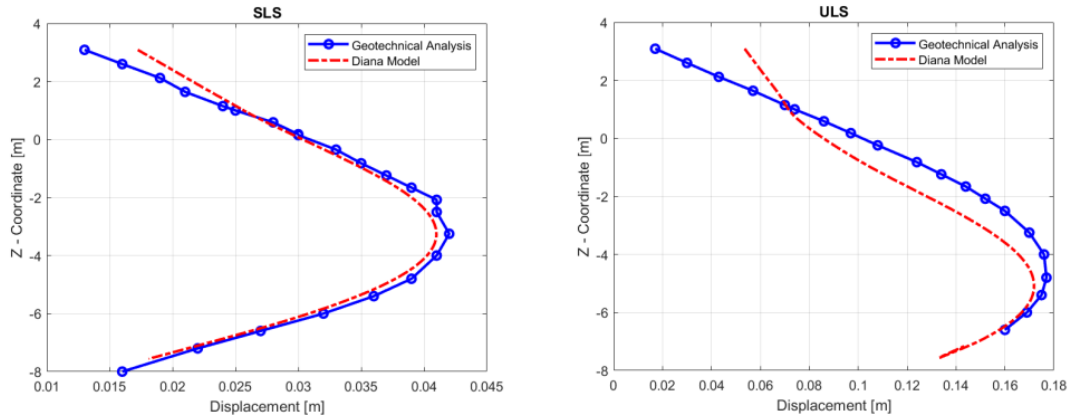

Figure 3.21: *Displacements of the sheet pile walls under SLS and ULS loading, Diana model and results from geotechnical analysis.*

3.4.5 FEM-modelling ALS

In this section it is described how the model is adjusted for the accidental load case. The accidental load case is capturing the behaviour of the system if one anchor gets damaged or broken, giving a double span length between anchors, resulting in increased stresses in the capping beam and a deformation as indicated in Figure 3.22 (left). As seen in the figure, the middle anchor is assumed to fail, whereas the nearby anchors, A & B, will have to carry additional loads.

Since the geotechnical analyses did not include the ALS loading case a calibration model was created in the software FEM-design, which was used for the model approach with prescribed deformations. In this model the entire sheet pile was included, with springs representing soil and anchors. The model was calibrated towards the SLS loading state from the geotechnical analysis and after that, the middle anchor was removed. The resulting displacements at the anchor location of this model, was then implemented into the FE-model in Diana. This was done by adapting the displacement ratio for each anchor relative to the middle one thus displacing each anchor in the ALS model as the calibrated FEM-design model.

One concern during modelling the ALS load case is if the loss of one anchor would largely influence the location of the zero moment section of the sheet pile wall. To the right in Figure 3.22 it is shown that this moment section does not change significantly if removing the middle anchor, why it is decided to keep a constant zero moment section for the FE-model in Diana.

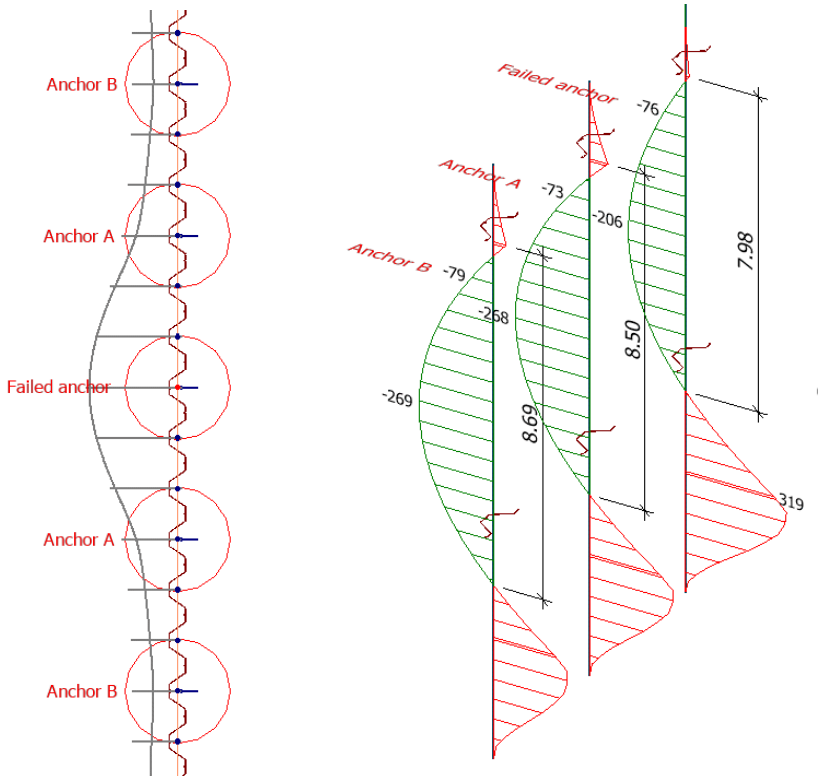

Figure 3.22: *Deformation of section in ALS load case with one anchor released at middle, top view (left). Moment distribution, middle failed anchor and the two outer anchors, A B next to it (right).*

4
Results

4.1 Results From the FEM-model

Analyses are performed for two models. One with conventional reinforcement according to the case study, and one model with a fiber reinforced capping beam extension, while conventional reinforcement in the capping beam is kept. For the SLS and ALS load cases results from both models are presented while for ULS results from the model with fiber reinforcement are presented. Since the concrete might crack under the characteristic load case or be subjected to thermal or shrinkage cracking, analyses presented for the coming sections have a reduced tensile strength. It is thus assumed that the concrete is fully cracked and tensile strength of concrete is set to 0.5 MPa. Results from the analyses with the mean tensile strength of concrete, 3.2 MPa, will be presented in appendices for the SLS load case.

4.1.1 Description of Output From Diana

The different used outputs for Diana are shortly described in this section. Outputs have been used in order to obtain values for stresses in concrete and reinforcement, displacements of the quay wall and in order to investigate the cracking of concrete. In Table 4.1 all the outputted data is described and the syntax for the output is stated. This syntax in Diana will be shown in all screenshot figures from the software as a description of what is displayed. Cracking of concrete is visualized through crack strains and crack widths output. Crack widths are automatically calculated in Diana as the crack bandwidth multiplied with the crack strain. Stresses in concrete are in the project mainly presented in terms of principal stresses. A separate shear component(S_{yz}) is however included in order to obtain results of the shear stress in the capping beam extension at the side close to the sheet piles.

Table 4.1: *Description of outputs and its syntax in Diana.*

Output Description	**Diana Syntax**
Stress principal dir.	S1, S2 ,S3
Crack width Principal dir.	Ecw1, Ecw2, Ecw3
Reinforcement stresses	SXX, SYY, SZZ
Crack strain	Eknn, Gknt, Gkns
Total strain, principal dir.	E1, E2, E3

4.1.2 Mesh Sensitivity Test

A mesh sensitivity analysis for the material models can be seen in Chapter 3.3.1.1.

4.2 Analysis in the Serviceability Limit State

In this section results from the analysis in the serviceability limit state are presented. To start off the overall displacements of the structure with and without the capping beam are shown. After that, the concrete beams are investigated with and without the fiber reinforcement. In this particular load case the crack widths and locations of cracks in concrete as well as the shear stresses in concrete close to the sheet piles, are of interest. For this section the analysis of the fully cracked capping beam will be presented. The analysis of the capping beam without reduced tensile strength of concrete can be seen in Appendix E.

4.2.1 Deformation of the Structure - SLS

For this section the difference in deformations between the models for the two different model approaches are compared. It can be seen from Figure 4.1 (right) that if modelling the structure with springs at the anchor locations, the capping beam and its extension is following the deformation of the sheet piles. Overall the displacements from this modelling approach is very similar, adding the capping beam does not change the displacements much compared to a waling beam. In Figure 4.1 to the left, the deformations from modelling the structure with a prescribed displacement on the anchors are displayed. The results show, a large difference in the deformed shape, compared to the prior modelling approach with springs. The concrete does not rotate as much and translates less.

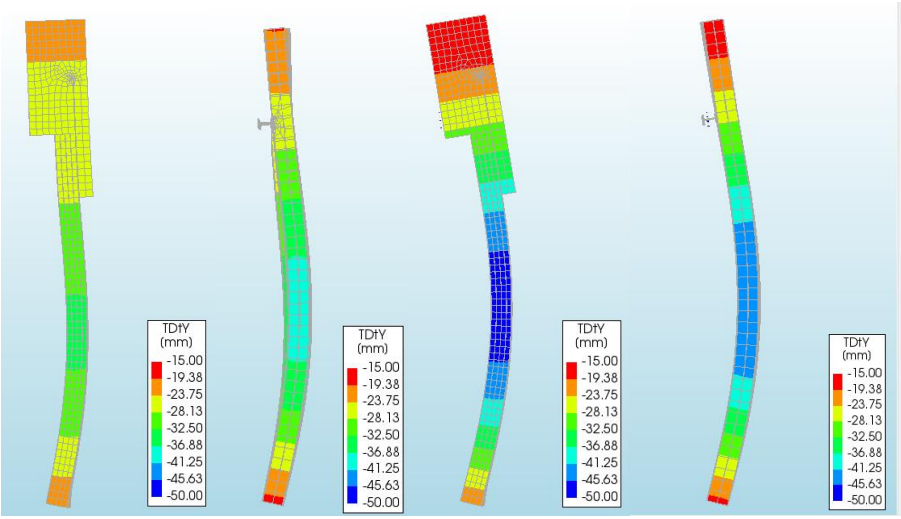

Figure 4.1: *Model with prescribed displacements on anchor plates to the left and with spring stiffnesses to the right.*

In Figure 4.2 out-of-plane displacements of both modelling approaches are shown with the waling beam attached. The figure shows that the model with prescribed displacements yields lower maximum displacements as well as a less uniform distribution. Since the model with prescribed displacements yields a larger difference in displacements between the anchors, this will result in more conservative results. This model further obtains displacements as expected in between the anchor locations and therefore it is chosen to go forward with this model for further results.

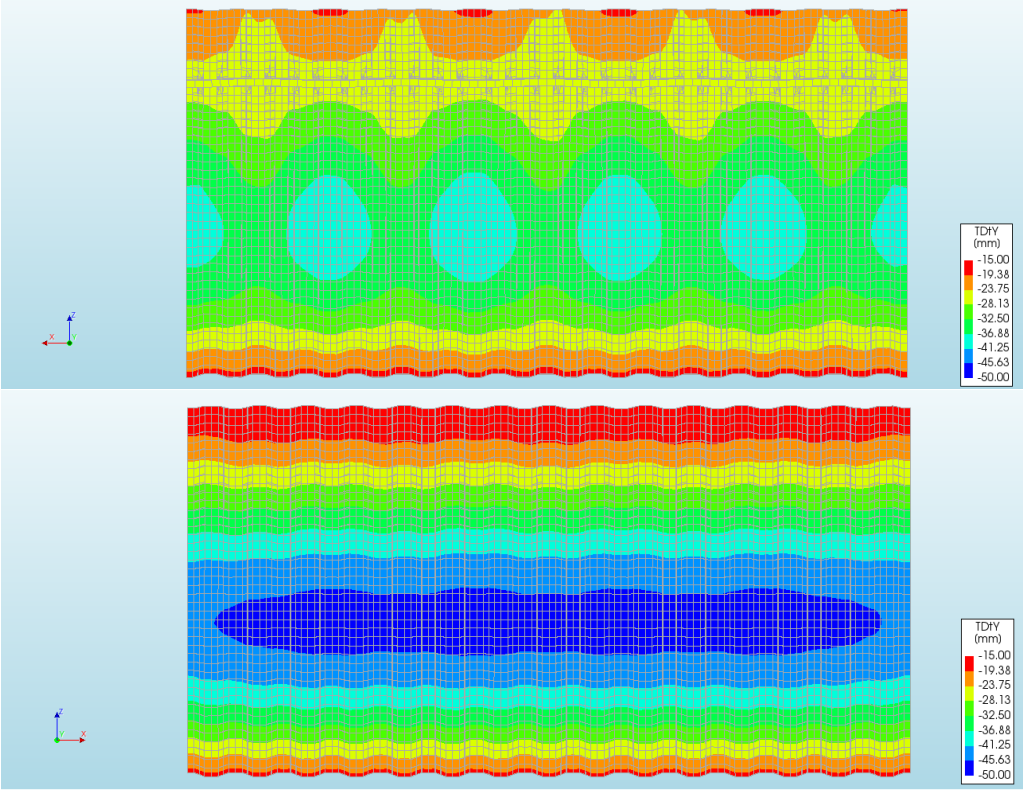

Figure 4.2: *Out-of-plane displacements of sheet piles with waling beam for both modelling approaches in service limit state. Model with prescribed displacements in the top and model with spring stiffnesses in the bottom.*

4.2.2 Principal Stress and Strain - SLS

In Figure 4.3 principal stresses in concrete are shown for the model containing a fiber reinforced capping beam extension. Total strains are shown in Figure 4.4 for the same model. The figures indicate that the largest stresses are located over the anchors, as well as in the capping beam extension. The results further show that the joint between the capping beam and the extension is a location where concentration of stresses can be seen.

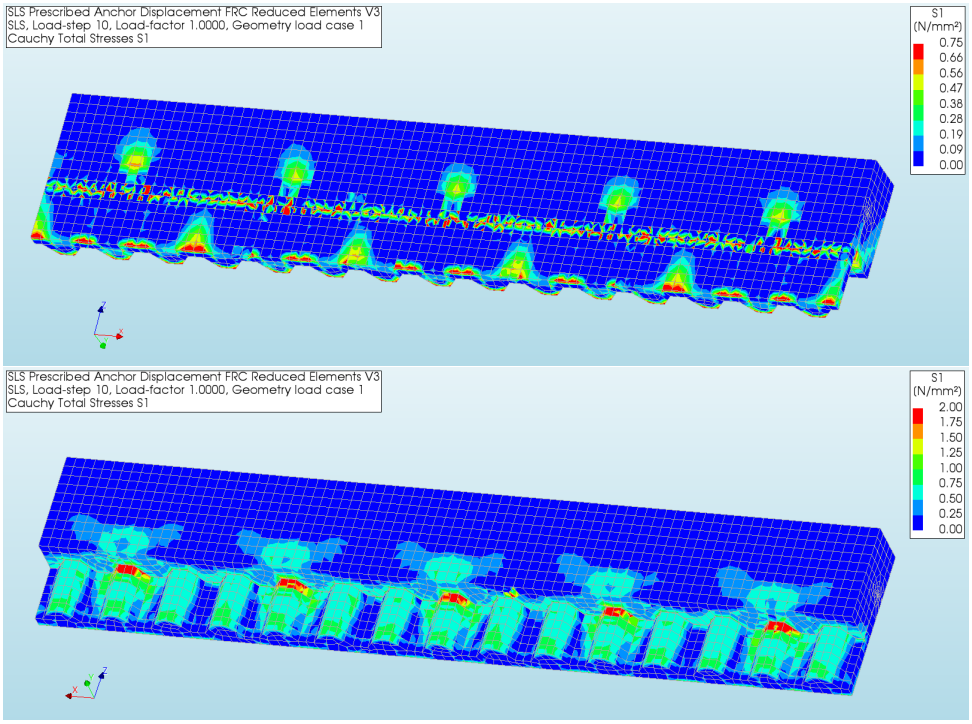

Figure 4.3: *Principal stress in service limit state, for front and back of capping beam for the model with fiber reinforced concrete. Maximum value, 2.3 MPa.*

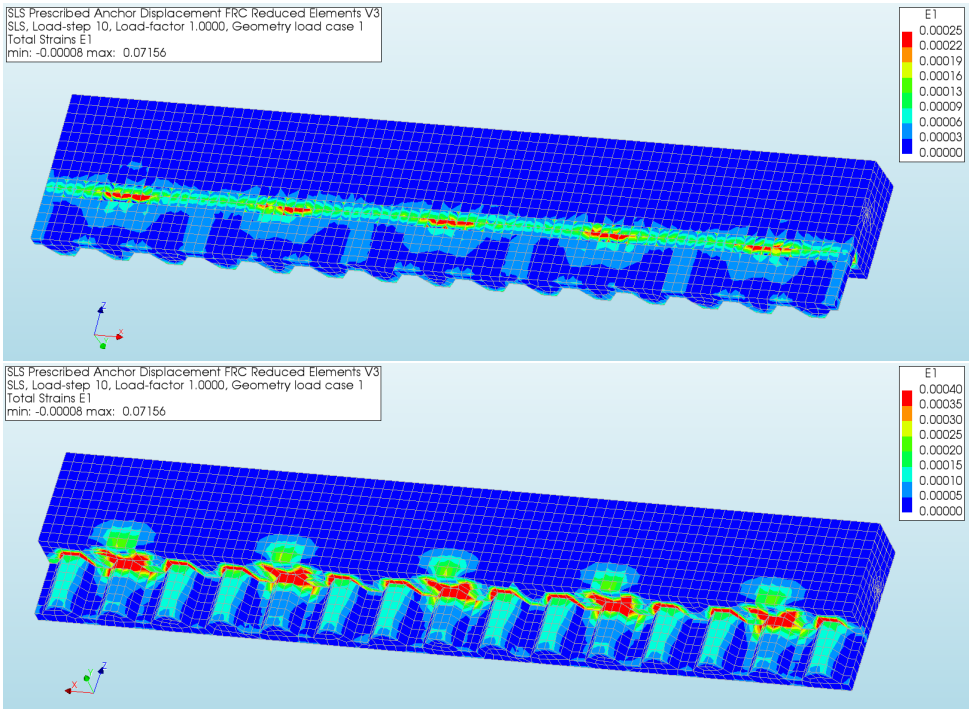

Figure 4.4: *Total Strain in service limit state, for front and back of capping beam for the model with fiber reinforced concrete. Maximum value front of capping beam 0.25 ‰.*

4.2.3 Crack Pattern & Crack Widths - SLS

The crack pattern of the model with conventionally reinforced concrete can be seen in Figure 4.5 and for the model with a fiber reinforced capping beam extension in Figure 4.6. These figures indicate that cracking takes place at the joint between the capping beam and the extension for both models. Cracking can also be seen close to the anchors in both models, but is more pronounced in the model with conventional concrete.

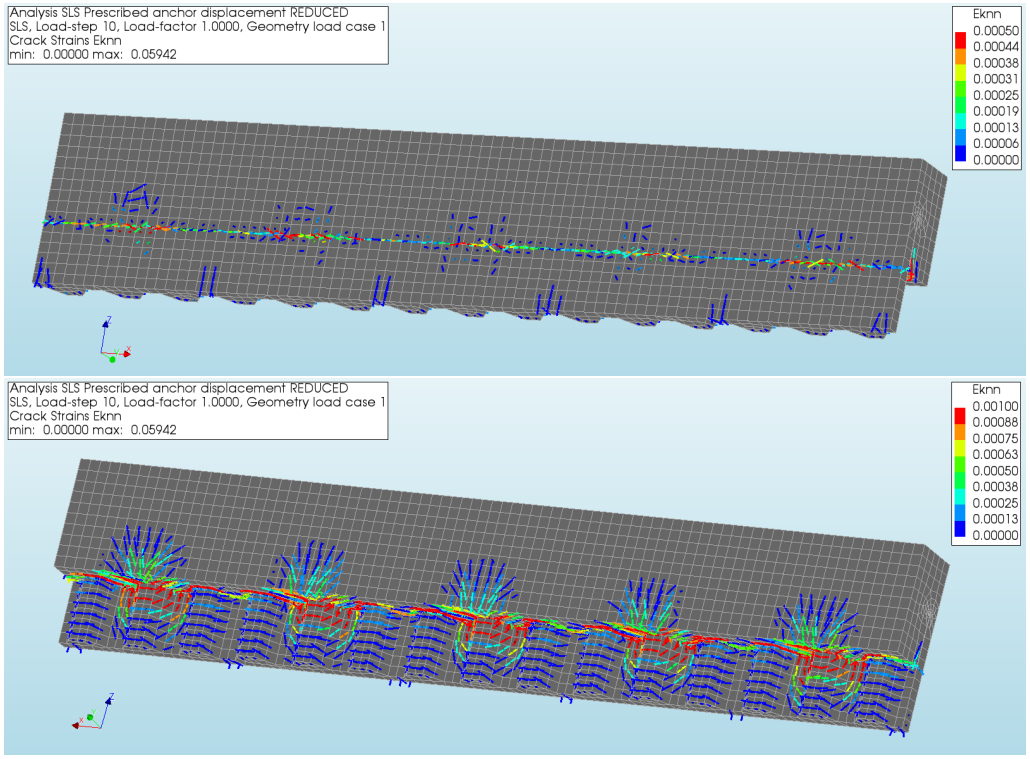

Figure 4.5: *Crack strains formed in serviceability limit state for the model with conventionally reinforced concrete. The front of the beam is showed in the top of the figure, and the backside of the beam in the bottom of the figure. Maximum strain front of capping beam 0.6 ‰.*

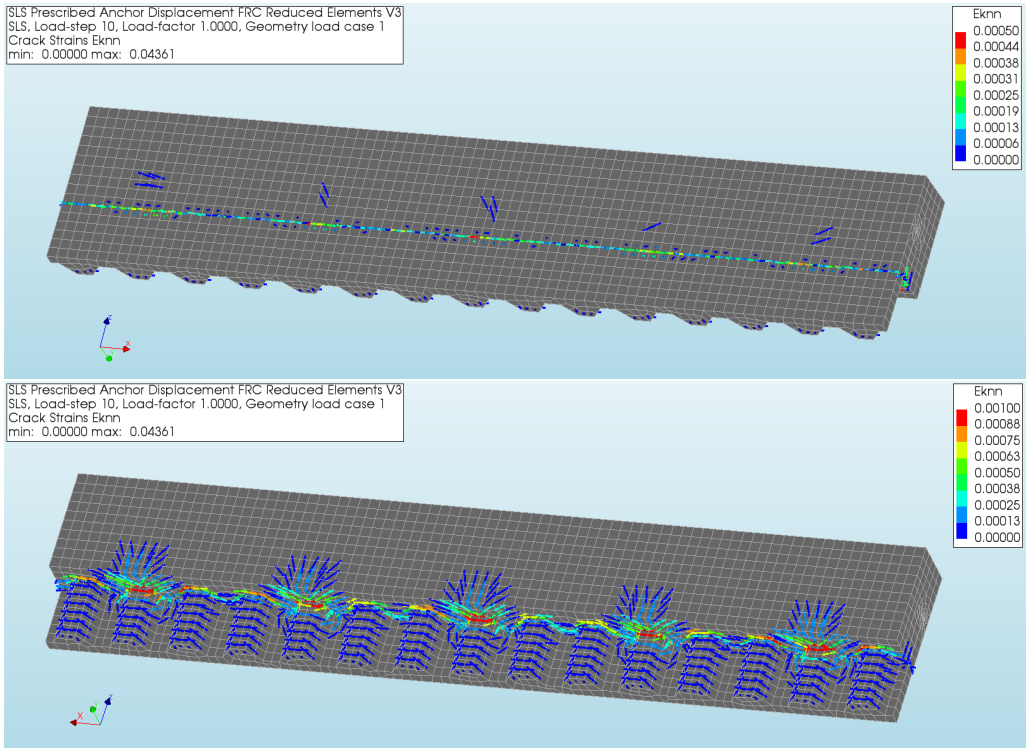

Figure 4.6: *Crack strains formed in serviceability limit state for the model with fiber reinforced concrete. The front of the beam is showed in the top of the figure, and the backside of the beam in the bottom of the figure. Maximum strain front of capping beam 0.6 ‰.*

Resulting crack widths can be seen in Figure 4.7, for the model containing fiber reinforcement in the capping beam extension. Surface cracks are very small and well below the limit of 0.2 mm. Largest crack widths can be observed close to the anchors. Crack widths for the model with conventionally reinforced concrete are shown in Figure 4.8. From the figures it can be seen that the conventionally reinforced model obtains more damage and larger crack widths.

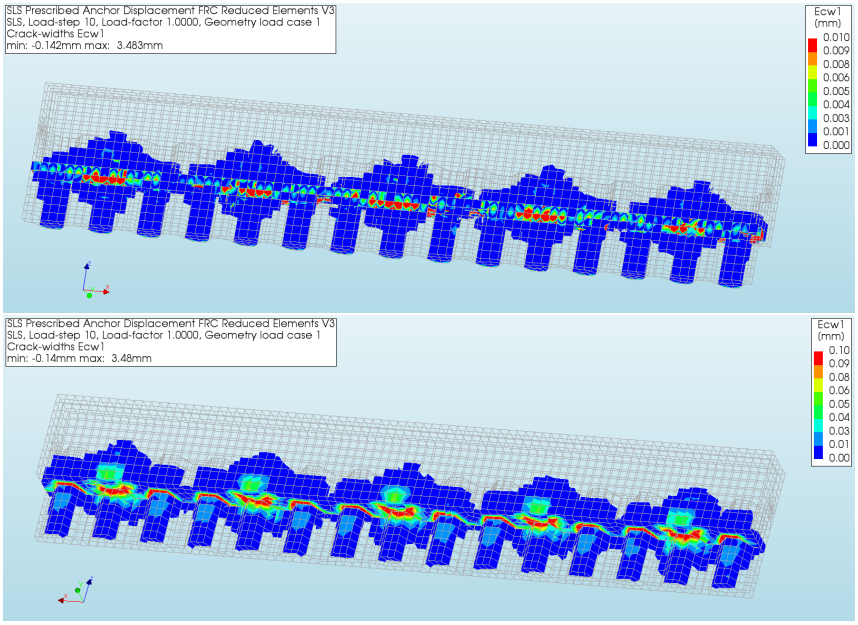

Figure 4.7: *Crack widths formed in serviceability limit state for the model with fiber reinforced concrete. The front of the beam is showed in the top of the figure, and the backside of the beam in the bottom of the figure. Max crack width on surface front 0.05 mm. Permitted crack width is 0.2 mm.*

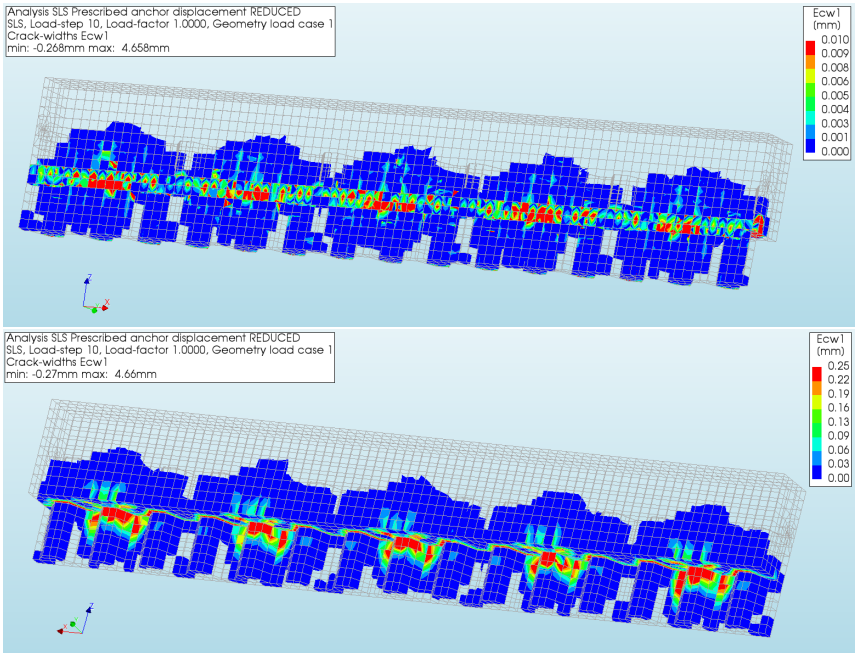

Figure 4.8: *Crack widths formed in serviceability limit state for the model with conventionally reinforced concrete. The front of the beam is showed in the top of the figure, and the backside of the beam in the bottom of the figure. Max crack width on surface front 0.06 mm. Permitted crack width is 0.2 mm.*

4.2.4 Shear Stress Between Concrete & Sheet Pile - SLS

From the literature study it has been suggested that the limit for the shear stress to break the adhesion between the steel and concrete is 0.75 MPa. In Figure 4.9 shear stresses for the capping beam extension can be seen. Results are indicating that for both conventionally and fiber reinforced concrete the recommended limit is reached indicating that adhesion is lost for several sections of the capping beam extension.

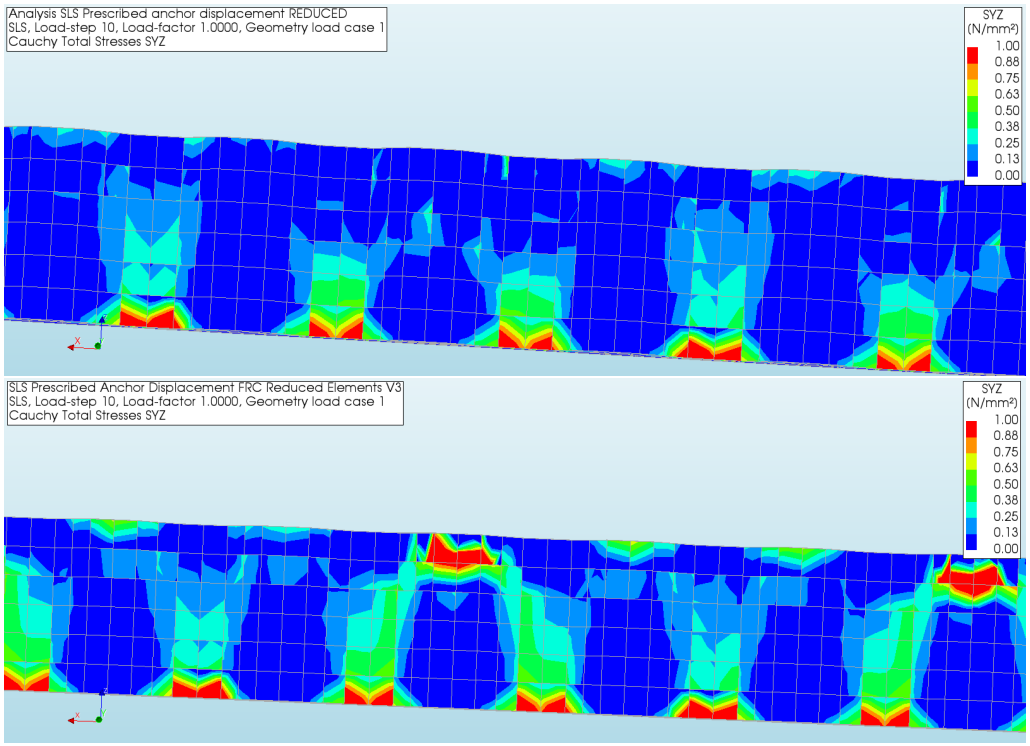

Figure 4.9: *Shear stress at backside of the capping beam extension in the service limit state for conventionally reinforced concrete (top) and fiber reinforced concrete (bottom). Max shear stress, conventionally reinforced: 0.89 MPa, FRC: 0.92 MPa.*

4.3 Analysis in the Accidental Limit State

For this section the results for the accidental load case are presented. The deformation of the structure and the damage to concrete has been included in the results in the coming sections.

4.3.1 Deformations - ALS

The deformed structure for the accidental limit state is shown in Figure 4.10. The structure experiences the highest displacement at the section of the removed anchor and the displacements are gradually decreasing towards the outer boundaries.

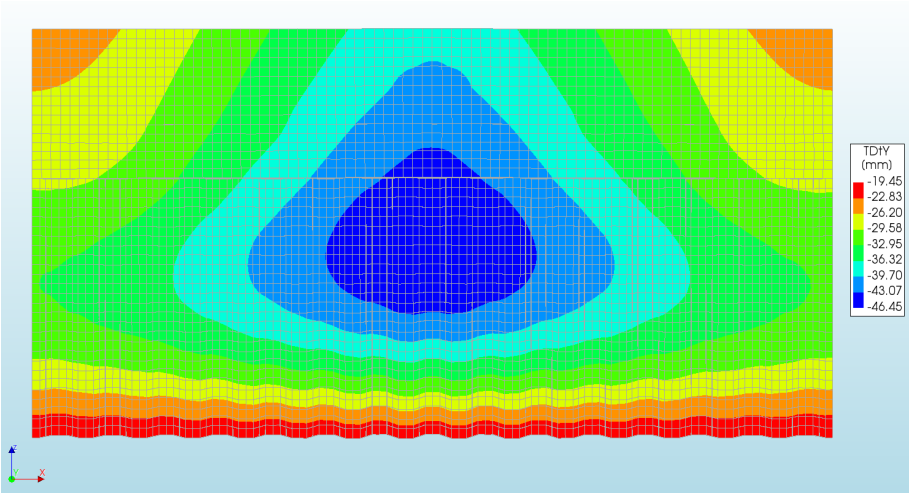

Figure 4.10: *Out-of-plane displacements in accidental limit state for the model with fiber reinforced concrete.*

4.3.2 Stresses & Strains - ALS

Crack strains for the model with a fiber reinforced capping beam extension in ALS can be seen in Figure 4.11. The figure shows that damage of concrete is concentrated towards the middle sections of the beam as well as in the backside of the capping beam extension. Cracking at the end sections of the beam is due to boundary conditions. Principal stresses in concrete are shown in Figure 4.12 for the fiber reinforced model. Crack strains and principal stresses for the conventionally reinforced model can be seen in Appendix F.

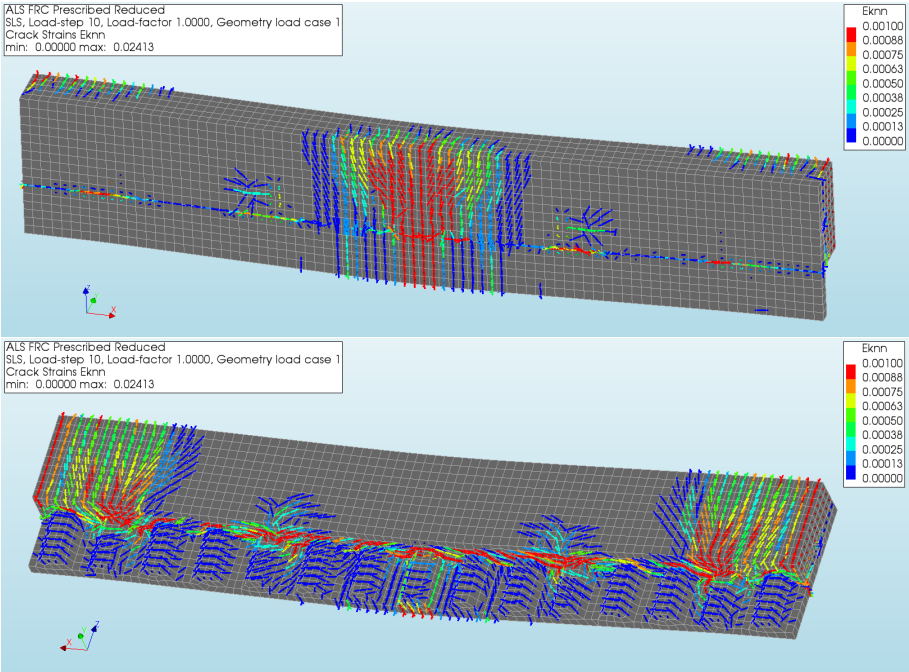

Figure 4.11: *Crack strains in the accidental limit state for the model with a fiber reinforced capping beam extension.*

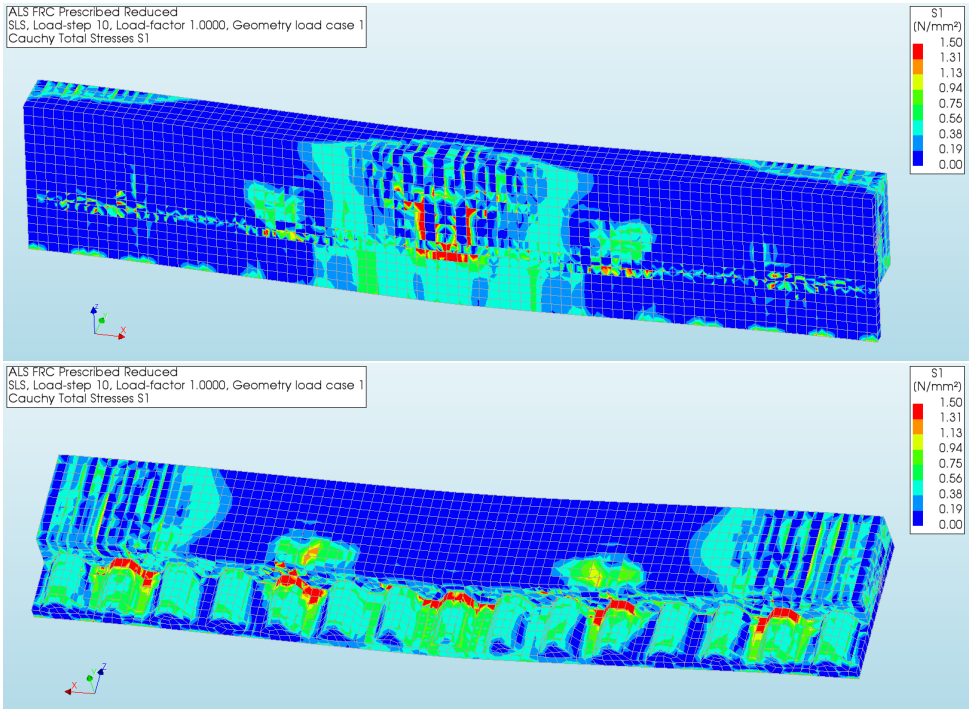

Figure 4.12: *Principal stress in concrete in the accidental limit state for the model with a fiber reinforced capping beam extension. Maximum value, 2.3 MPa.*

Total strains, limited to the ultimate residual tensile strain of fiber reinforced concrete, can be seen in Figure 4.13. Concentrations of strains are located towards the middle of the capping beam extension, but are below the ultimate strain of fibers (0.0096) in the capping beam, indicating that no brittle failure is expected in this load case. Total strains of the model with conventionally reinforced concrete can be seen in Figure 4.14.

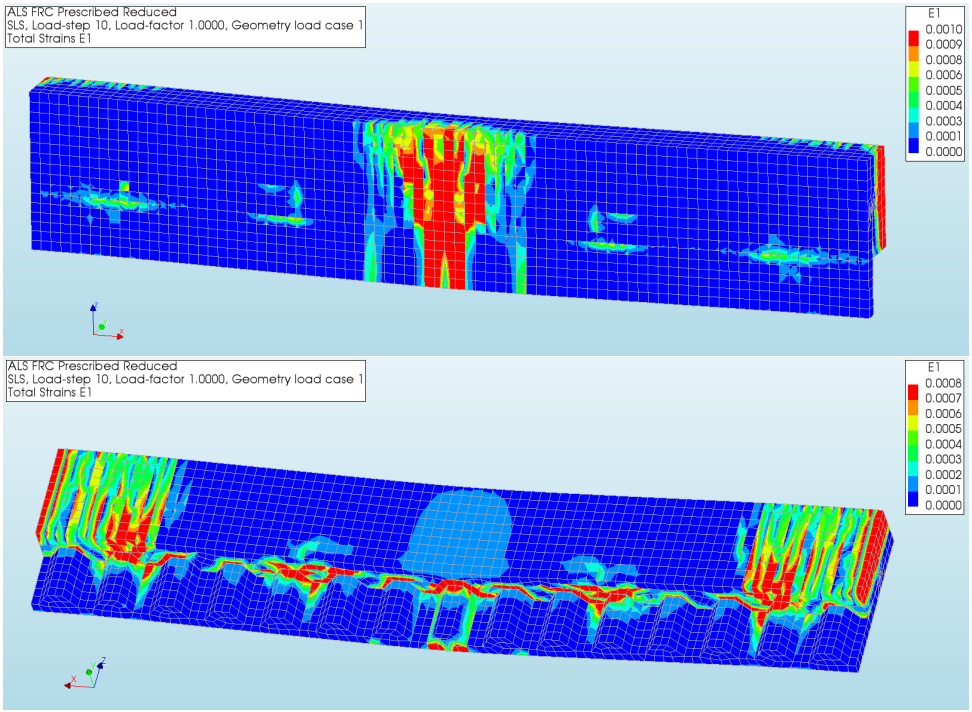

Figure 4.13: *Total strains in accidental limit state for the model with a fiber reinforced capping beam extension. Ultimate residual tensile strength of the fiber is 9.6 ‰.*

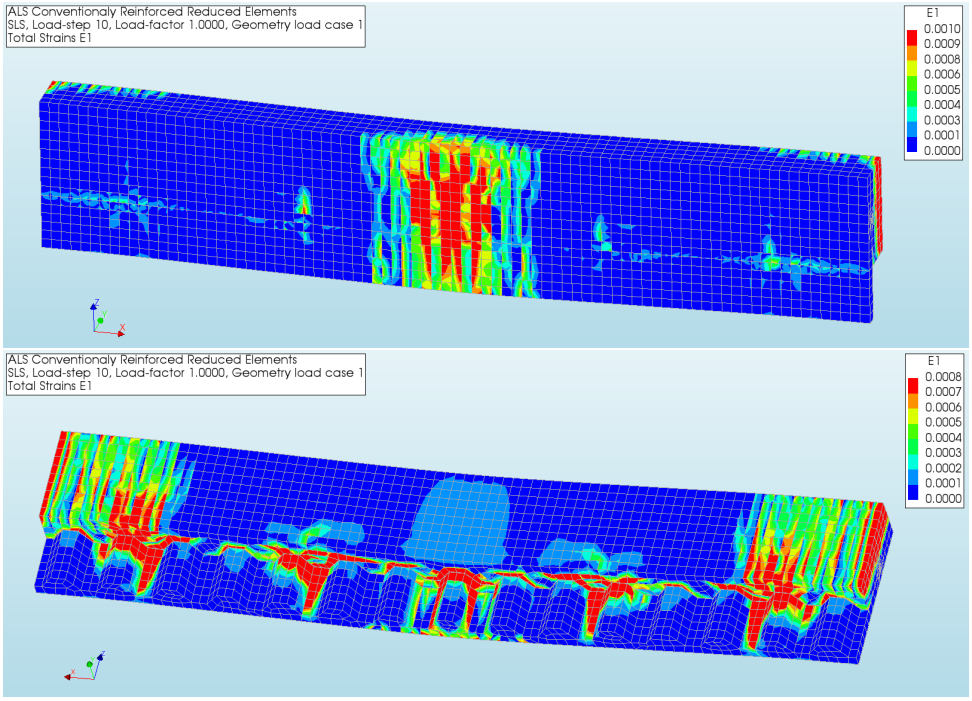

Figure 4.14: *Total strains in accidental limit state for the model with a conventionally reinforced capping beam. Ultimate residual tensile strength of the fiber is 9.6 ‰.*

4.3.3 Reinforcement Stresses - ALS

Reinforcement stresses can be seen in Figure 4.15 with maximum values reported in Table 4.2.

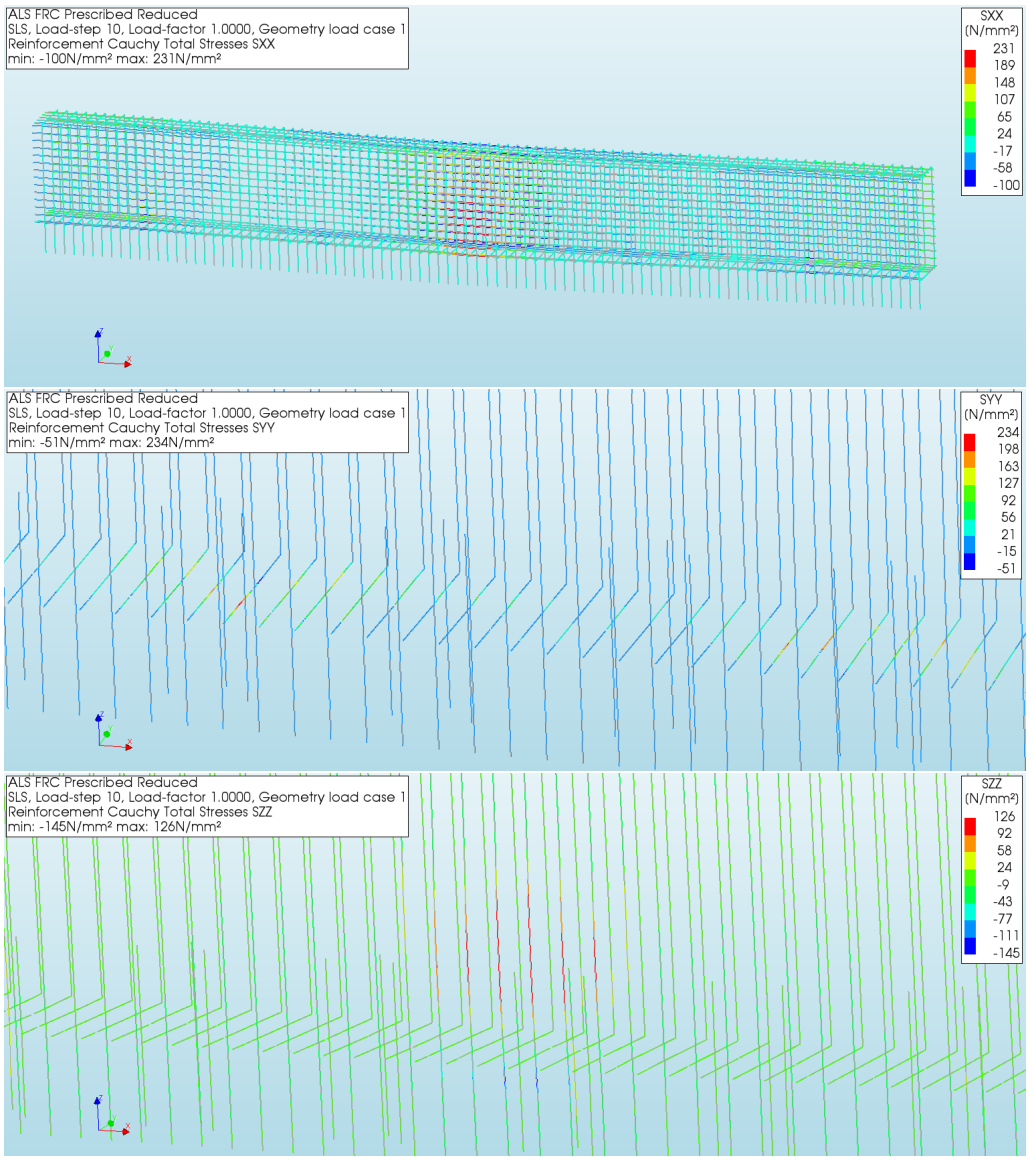

Figure 4.15: *ALS reinforcement stresses, for the model with fiber reinforced concrete, in x-, y- and z-direction.*

Table 4.2: *Maximum reinforcement stress in x-, y- and z-direction, for both models. Yield stress of reinforcement is 500 MPa.*

Reinforcement Dir.	FRC [MPa]	Conv. Reinforced [MPa]
X	231	201
Y	234	273
Z	126	131

4.4 Analysis in the Ultimate Limit State

In this section the results from the analysis in the ultimate limit state are presented when the structure is loaded by surcharges and by soil in failure.

4.4.1 Total Strain - ULS

The total strains for the ULS model are shown in Figure 4.16, for the model with conventional reinforcement. It can be seen that strains are concentrating over the anchor positions as well as at the interface between the concrete and steel for the backside of the capping beam extension.

For the model containing fiber reinforcement the total strains in the capping beam extension are shown in Figure 4.17, indicating that residual tensile strengths of fibers (0.0096) are not reached.

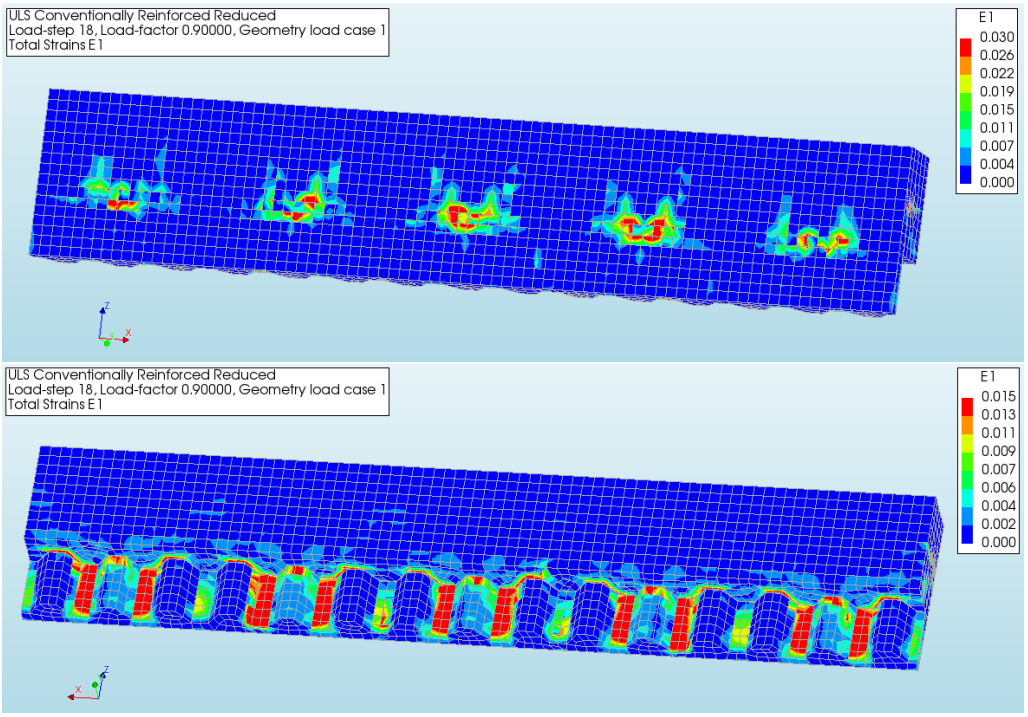

Figure 4.16: *Total Strain in ultimate limit state for the capping beam model with the conventionally reinforced concrete.*

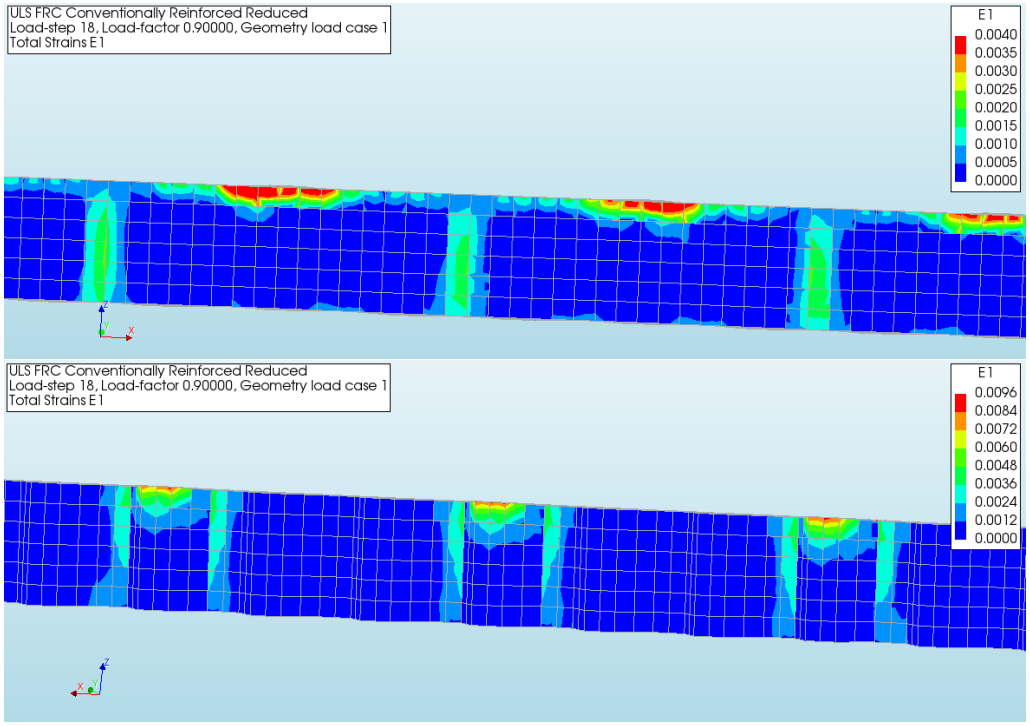

Figure 4.17: *Total Strain in ultimate limit state for the capping beam model with the fiber reinforced concrete. Maximum value, 6 ‰.*

4.4.2 Total Reinforcement Stress - ULS

In Figure 4.18 the reinforcement stress is shown for the ultimate limit state load case, both for the longitudinal and the vertical bars. Maximum stress in reinforcement in y-direction can be seen at the bars that are located at the lower part of the capping beam. The longitudinal stresses are low with peak levels at the location of the anchors. Stresses in reinforcement bars are overall low in the capping beam, indicating that the capping beam can carry more load until failure of reinforcement.

For the capping beam extension it can be seen that some reinforcement crossing both beams are experiencing high stresses in z-direction (lower right of Figure 4.18). Maximum reinforcement stresses are shown in Table 4.3 where it can be seen that the stresses in z-direction exceeds the yield stress of the reinforcement bars, strains are however below the maximum allowed strain in the steel, 0.075.

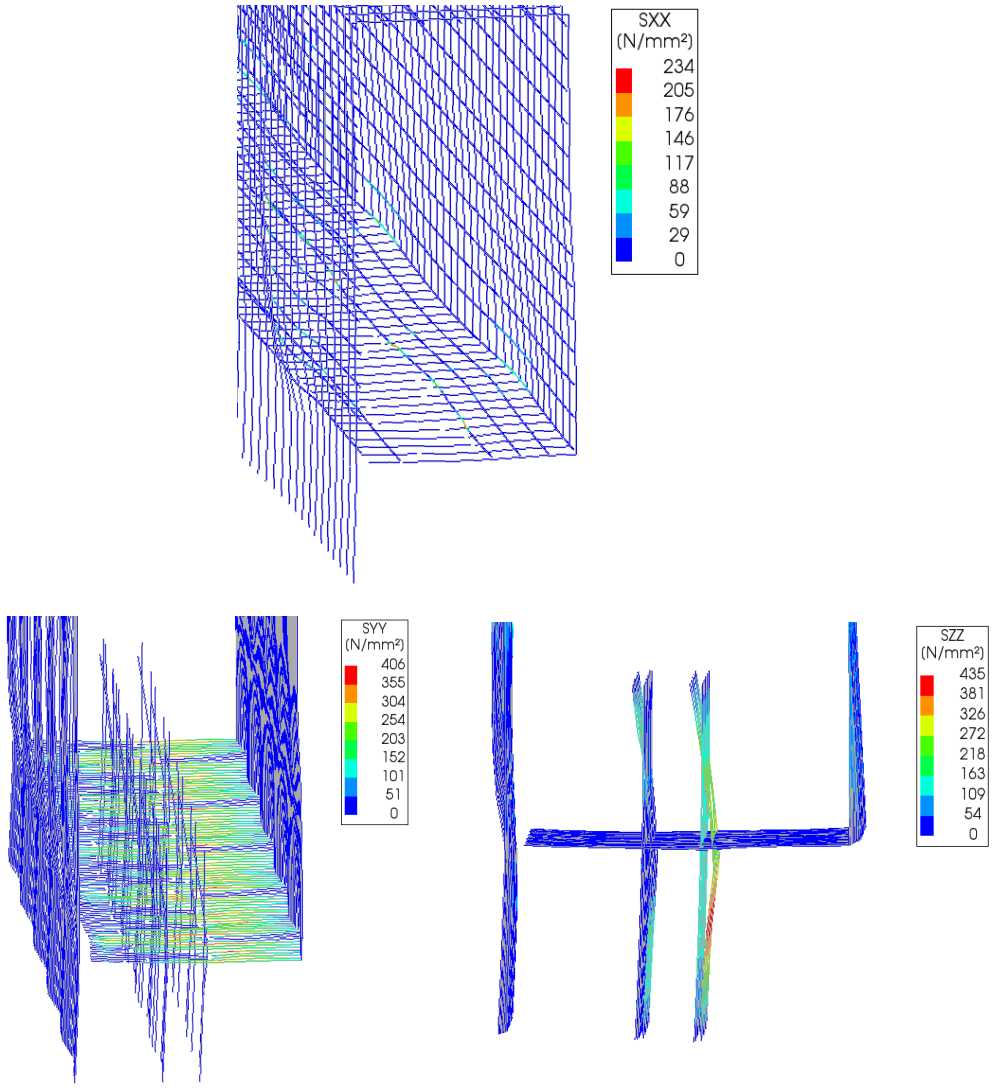

Figure 4.18: *ULS reinforcement stresses for the model with fiber reinforced concrete in x-, y- and z-direction.*

Table 4.3: Maximum reinforcement stresses in x-, y- and z-direction. Yield stress is 435 MPa.

Reinforcement Dir.	**Max. Reinf. Stress [MPa]**	**Max. Strain**
X	234	-
Y	406	-
Z	435	0.004

4.5 Hand Calculations

In this chapter hand calculations and results from the FE-model are compared. For the hand calculations, support and span strains of a linear elastic analysis of a continuous beam are compared to the results from the FE-model. The comparison is performed in the serviceability limit state, with characteristic tensile strengths for concrete. The concrete is mainly uncracked for this load case in the FE-model, which simplifies calculations. Hand calculations can be seen in Appendix G.

The results are indicating that the FE-model is yielding large peak values that are appearing locally over the anchors and in mid-span. In order to get similar results for hand calculations only a small part of the beam width should be considered. For example it is shown from results that strains in concrete, in the lower part of Figure E.2, are concentrated over the anchor and down into the capping beam extension and that only a small width of the beam is active. The total beam width is approximately 4 meters, while results show that only about 350 mm should be considered in order to obtain results within the same order of magnitude for hand calculations. Since stresses are dispersing into both the capping beam and its extension, an average height of these two parts has been used in calculations. In Table 4.4 below the total strains are presented at support and in span for both hand calculations and the FE-results. For clarification of the effective beam width and average beam height, see Figure 4.19.

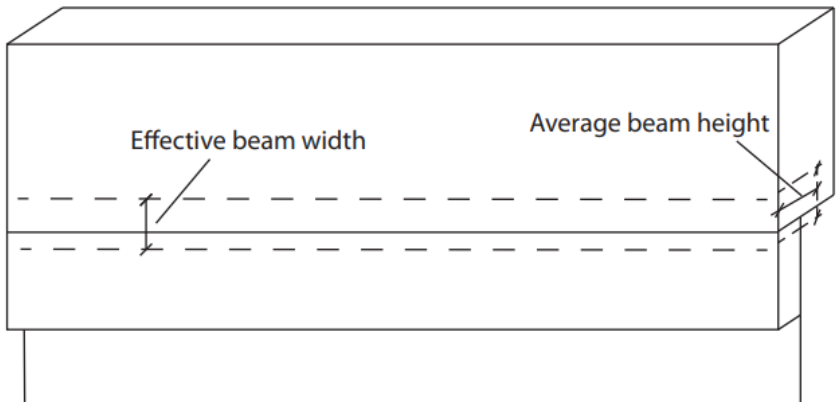

Figure 4.19: *Illustration of the assumptions of an effective beam width and an average beam height used in hand-calculations.*

Table 4.4: *Resulting strains from hand calculations and FE-analysis with corresponding differences.*

	Strain - Hand Cal. $[\cdot 10^{-4}]$	**Strain - FEM** $[\cdot 10^{-4}]$	**Difference** [%]
Span	1.0	1.0	1
Support	2.0	1.4	30

5

Conclusion & Recommendations

5.1 Conclusion

It can be concluded from all load cases that the most stressed part of concrete is at the anchor locations as well as at the intersection between the capping beam and its extension. The results are however indicating that the damage in the capping beam extension is small under the serviceability limit state loading and crack widths are generally kept small. The SLS results show that the crack widths could be limited below the critical values with the proposed fiber, which possesses a low residual tensile strength. It can further be noticed from Figure 4.7 & 4.8 that the model with a fiber reinforced capping beam extension obtains less damage and smaller crack widths.

It can further be noted from Figure 4.9 that the interface between concrete and the sheet pile wall is critical. According to the results the critical value of the shear stress, 0.75 MPa, stated in the literature study, see Chapter 2.3.3, is reached for some parts of the extension under the serviceability limit state loading. As this connection is critical in order to ensure that sheet piles are protected from corrosion and ensure safety of the structure, it is concluded that shear connectors of some kind are needed at this interface of materials.

For the ALS loading scenario the ultimate residual strains of fibers are not reached in the capping beam extension, see Figure 4.13, indicating that there is no brittle failure. In reinforcement the maximum stresses are at 200-300 MPa, which is far from the yield stress of 500 MPa.

In the ULS loading scenario the capping beam experiences concentrations of tensile stresses over the anchors as well as in the joint between the capping beam and its extension. From several Figures, for example 4.18, it is clear that this joint between the concrete beams is critical and it could further be concluded that reinforcement bars crossing both beams are of great importance in order to prevent separation and to limit crack widths. From reinforcement results it can also be concluded that bars crossing the sheet piles experience high stresses and are important to keep in the design. From the ULS results it can further be concluded that the residual strain of fibers is not reached for the model with fiber reinforcement.

A design method was presented in the literature study where the anchor force is

obtained from a geotechnical sheet pile calculation. This force is then assumed to act as a distributed load on the capping beam that is simply supported by anchors. From performed hand calculations it has been seen that in order to get similar results to the FE-model only an effective width should be used. This indicates that only a certain portion of the beam possesses a beam behaviour while other parts of the beam are not effective in load carrying. It is therefore important in design to consider the accounted beam width with care.

Even though the obtained results indicates that the capping beam extension with fiber reinforced concrete performs sufficiently and that a lot of reinforcement in the extension part could be removed, it should be noted that the proposed design is not following the recommendations from the Swedish standard on fiber concrete, as stated in Chapter 2.1.3. According to the Swedish standard, steel fibers used in the exposure class of this structure must be accompanied with bar reinforcement while synthetic fibers are not allowed for load carrying purposes in ULS.

5.2 Discussion and Recommendations for Further Research

One of the major difficulties during this thesis has been setting up a structural model in Diana of a problem that involves lots of geotechnics. For example it has been needed to allow the entire model to be able to translate, as the soil is not rigid. The finite element program Diana was mainly chosen since it offers advanced finite element modelling of reinforced concrete structures which has been the focus of the thesis. Taking more geotechnical aspects into account would have yielded a more realistic model, but the complexity of the model would have highly increased.

Since all modelling is performed for one project it raises concerns of how the specific geometry is connected to the results and how anchor positions and site conditions influence the results. Since the results are indicating that only a small part of the capping beam is active under loading and that stress concentrations appear over the anchors, the anchor position could highly influence the stresses in the capping beam extension. A high placement of anchors would then yield lower stresses in the capping beam extension.

The results from hand calculations are showing that only a certain width of the capping beam is effective during loading, which suggests that a topic for further research is finding criteria, based on for example geometry, that helps the designer to choose an appropriate effective width.

Due to time constraints there are load cases that have not been investigated during this thesis. Important load cases that would be of interest for further modelling are fender and bollard actions, which could pose damage to the capping beam.

Using non corroding fibers, such as synthetic fibers, can be of great interest to remove the risk of corrosion. However, synthetic fibers are for example sensitive to creep and their creep behaviour needs to be further investigated in order to fully ensure a safe use of this material.
According to research cited in the literature review, it was found that steel fibers possess high resistance to corrosion inside the concrete mixture and it may be of more practical interest to use steel fibers, since these fibers are the most commonly used. If more research is conducted on the subject of corrosion of steel fibers the application within industry can be used more. It often takes a long time for new solutions to be implemented in design codes and hopefully it can be used in the future.

Bibliography

Akcay, B. (2012). Experimental investigation on uniaxial tensile strength of hybrid fibre concrete. *Composites Part B: Engineering*, *43*(2), 766–778. https://doi.org/10.1016/j.compositesb.2011.08.017

Alexander, M. G. (2016). *Marine concrete structures: Design, Durability and Performance*.

Bentur, A., & Mindess, S. (2006). *Fibre Reinforced Cementitious Composites*. https://doi.org/10.1201/9781482267747

Berthet, J. F., Yurtdas, I., Delmas, Y., & Li, A. (2011). Evaluation of the adhesion resistance between steel and concrete by push out test. *International Journal of Adhesion and Adhesives*, *31*(2). https://doi.org/10.1016/j.ijadhadh.2010.11.004

Bradford, D. J. O., & A., M. (1995). *Composite Steel and Concrete Structural Members*. https://doi.org/10.1016/c2009-0-08012-x

Broeken, J. d. G. M. (2014). *Quay Walls, Second Edition* (2nd Editio). CRC Press/Balkema.

Carl A. Thoresen. (2010). *Port Designer's Handbook*. Thomas Telford Limited.

CEB. (2010). CEB-FIP Model Code 2010. *fib Model Code for Concrete Structures 2010*.

Chernov, V., & Buslov, V. (2004). Protection and repairs of steel sheet piles in tidal zone. *Port Development in the Changing World, PORTS 2004, Proceedings of the Conference*. https://doi.org/10.1061/40727(2004)94

Degée, H., Dragan, D., Bogdan, T., & Plumier, A. (2017). Transfer of the longitudinal shear at the steel-concrete interface in concrete members reinforced by steel profiles. *High Tech Concrete: Where Technology and Engineering Meet - Proceedings of the 2017 fib Symposium*. https://doi.org/10.1007/978-3-319-59471-2{_}126

DIANA FEA. (2021). Diana User's Manual. https://dianafea.com/diana-manuals

Domone, M. S. P. (2018). *Construction Materials - Their Nature and Behaviour*. Taylor & Francis Group.

Löfgren, I. (2005). Fibre-reinforced concrete for industrial construction - A fracture mechanics approach to material testing and structural analysis. *Doktorsavhandlingar vid Chalmers Tekniska Hogskola*, (2378).

Marcos-Meson, V., Michel, A., Solgaard, A., Fischer, G., Edvardsen, C., & Skovhus, T. L. (2018). Corrosion resistance of steel fibre reinforced concrete - A literature review. *Cement and Concrete Research*, *103*(October 2017), 1–20. https://doi.org/10.1016/j.cemconres.2017.05.016

Minelli, F., Tiberti, G., & Plizzari, G. (2011). Crack control in RC elements with fiber reinforcement. *American Concrete Institute, ACI Special Publication*, (280 SP), 76–93.

Noushini, A., Samali, B., & Vessalas, K. (2013). Effect of polyvinyl alcohol (PVA) fibre on dynamic and material properties of fibre reinforced concrete. *Construction and Building Materials*, *49*, 374–383. https://doi.org/10.1016/j.conbuildmat.2013.08.035

PEAB (technical report). (2021).

Plos, M. (2000). Finite element analyses of reinforced concrete structures.

Silfwerbrand, J. (2020). Fiberbetong - ett kapitel för sig. *Betong*, *5*. https://betong.se/2020/10/31/fiberbetong-ett-kapitel-for-sig/

SIS (Swedish Standards Institute). (2005). SVENSK STANDARD SS-EN 1992-1-1:2005. *SS-EN 1992-1-1:2005*, (138227).

SIS (Swedish Standards Institute). (2007). Eurocode 3:Design of steel strectures - Part 5: Piling. *SS-EN 1993-5:2007*.

SIS (Swedish Standards Institute). (2018). Svensk Standard. *SS 812310:2014*, 24.

Swedish standards Institute. (2006a). Svensk standard: Fibrer för betong – Del 1 : Stålfibrer – Definitioner , specifikationer och överensstämmelse (Fibres for concrete – Part 1 : Steel fibres – Definitions , specifications and conformity). *Ss-En 14889-1:2006*, *1*.

Swedish standards Institute. (2006b). Svensk standard: Fibrer för betong – Del 2: Polymerfibrer – Definitioner, specifikationer och överensstämmelse. *Ss-En 14889-2:2006*, *1*.

Tsinker, G. P. (1995). *Marine Structures Engineering: Specialized Applications*. https://doi.org/10.1007/978-1-4615-2081-8

Tsinker, G. P. (1997). *Handbook of Port and Harbor Engineering*. https://doi.org/10.1007/978-1-4757-0863-9

Wells, J. (2010). Design of capping beams. *Structural Engineer*, *87*(23-24), 23–26.

Zhang, P., Han, S., Ng, S., & Wang, X. H. (2018). Fiber-Reinforced Concrete with Application in Civil Engineering. *Advances in Civil Engineering*, *2018*. https://doi.org/10.1155/2018/1698905

A

Appendix A

Calculation of crack spacing and crack widths for verifying the FE-model. Equations and parameters according to Eurocode SS-EN 1993-1-1:2005

Crack Spacing

$\phi := 20mm$ Bar diameter

$a := 120mm$ Side length

$c := \frac{a - \phi}{2} = 0.05\,m$ Concrete cover

$k_1 := 0.8$ Good Bonding

$k_2 := 1.0$ Pure Tension

$k_3 := 7 \cdot \frac{\phi}{c} = 2.8$ From National Annex

$k_4 := 0.425$ Rec. value

$A_s := \phi^2 \cdot \frac{\pi}{4} = 314.159 \cdot mm^2$ Steel area

$A_{c.eff} := a^2$ Effective Concrete Area

$\rho_{p.eff} := \frac{A_s}{A_{c.eff}} = 0.022$ Reinforcement amount

$S_{rmax} := k_3 \cdot c + k_1 \cdot k_2 \cdot k_4 \cdot \frac{\phi}{\rho_{p.eff}} = 0.452\,m$ **Max crack spacing EC**

$S_{rm} := \frac{S_{rmax}}{1.7} = 0.266\,m$ **Average Crack Distance**

Figure A.1: Calculations of crack spacing for the tension stiffening test.

Crack Widths

$\phi := 20mm$ Reinforcement diameter

$E_s := 200GPa$ Youngs Modulus steel

$E_c := 34GPa$ Youngs Modulus, C 35 / 45

$f_{ctm} := 3.2MPa$ Mean tensile strength, C 35/45

$\sigma_s := 250MPa$ Reinforcement Stress
Taken from Diana

$k_t := 0.6$ Short Term Loading

$f_{ct.eff} := f_{ctm}$ Mean tensile strength when first crack appears

$\alpha_e := \frac{E_s}{E_c} = 5.882$ Stiffness ratio

Strain difference Concrete and reinforcement

$$\Delta\varepsilon_m := \frac{\sigma_s - k_t \cdot \frac{f_{ct.eff}}{\rho_{p.eff}} \cdot \left(1 + \alpha_e \cdot \rho_{p.eff}\right)}{E_s} = 7.535 \times 10^{-4}$$

$$\Delta\varepsilon_m \geq 0.6 \frac{\sigma_s}{E_s} = 1$$

$$0.6 \frac{\sigma_s}{E_s} = 7.5 \times 10^{-4}$$

$w_k := S_{rmax} \cdot \Delta\varepsilon_m = 0.34 \cdot mm$ **Characteristic crack width EN 1992 -1 -1**

$w_{k.mean} := S_{rm} \cdot \Delta\varepsilon_m = 0.2 \cdot mm$ **Mean crack width EN 1992 -1 -1**

Figure A.2: Calculations of crack widths for the tension stiffening test.

B

Appendix B

Total strain crack Model	uniaxial residual strength	uniaxial residual strain
	5 MPa	0.576
	2.2 MPa	0.0876
	1 MPa	0.18
Uniaxial tensile strength	7.5 MPa	
Young's modulus	36.6 GPa	
Poisson's ratio	0.15	
Mass density	2502 kg/m^3	
Compressive strength	60 MPa	
Compressive curve	Ideal	
Crack orientation	rotating	
Multi-directional fixed crack model		
Uniaxial tensile strength	7.5 MPa	
Young's modulus	36.6 GPa	
Poisson's ratio	0.15	
Tension cut off	Constant Stress cut of	
Tension softening	Multi-linear	
Shear retention	Full shear retention	

Table B.1: Material parameters tensile test for total strain and multi-directional fixed crack models

Material data based on experimental data from test on size M specimen of mix 2 is represented in Table B.1. The stress-strain data used for the multi-directional crack model corresponds to the yellow line in Figure 3.10. For the total strain based model the uniaxial residual strength and the uniaxial residual strain is identified for three stages of the crack propagation given in Table B.1.

C

Appendix C

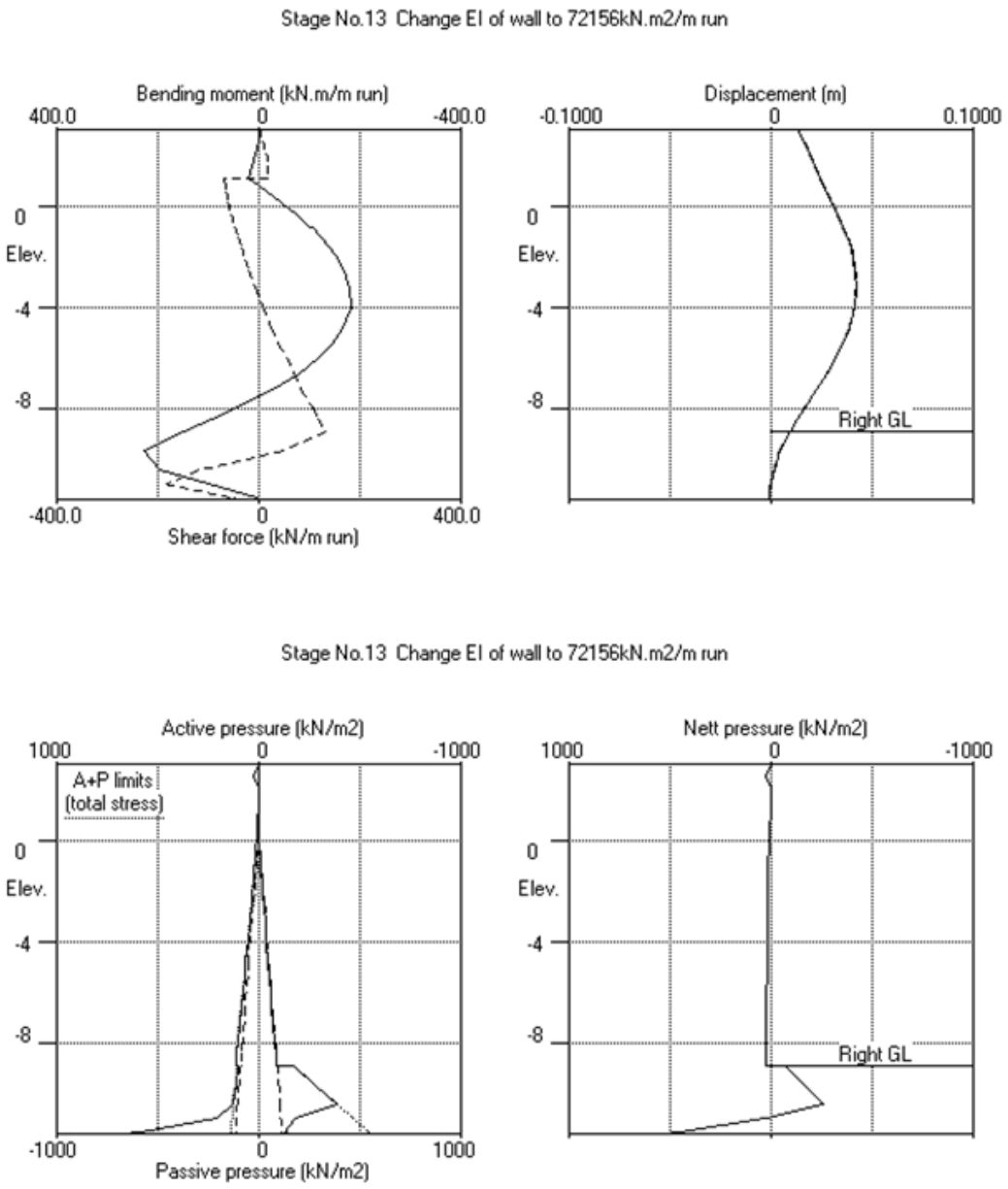

Figure C.1: Geotechnical analyses used as reference for the serviceability limit state load case. Showing bending moment, shear force, displacements and soil pressures.

D

Appendix D

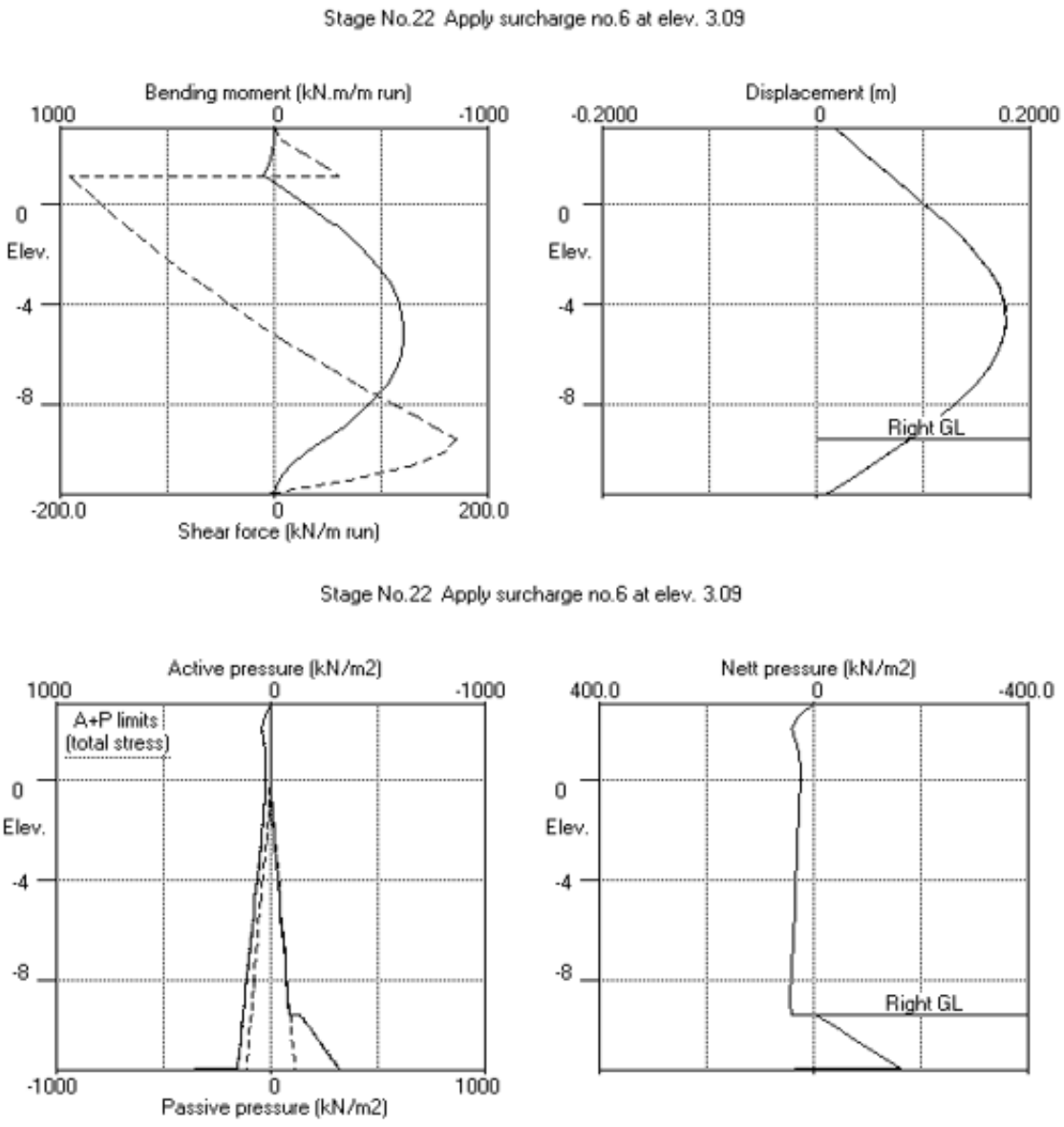

Figure D.1: Geotechnical analyses used as reference for the ultimate limit state load case. Showing bending moment, shear force, displacements and soil pressures.

E

Appendix E

Serviceability limit state analysis with a tensile strength of concrete of 3.2 MPa.

Principal tensile stress in Figure E.1 and total strain in Figure E.2 for the fiber reinforced model. For the conventionally reinforced model, stresses and strains in concrete are shown in Figure E.3 & E.4 respectively.

Crack widths for both the model containing fiber reinforcement and the model containing conventional reinforcement can be seen in Figure E.5 & E.6 respectively.

Shear stresses in concrete at the surface close to the sheet piles are shown in Figure E.7 & E.8 for the conventionally and fiber reinforced models respectively.

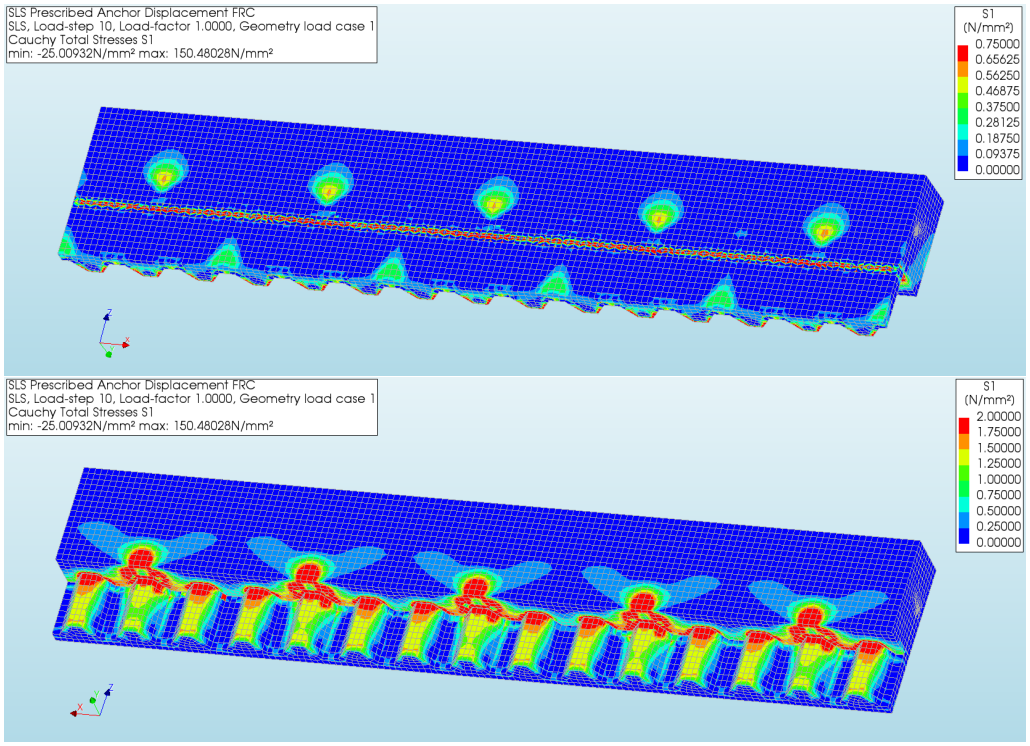

Figure E.1: *Principal stress in service limit state, for front and back of capping beam, fiber reinforced concrete.*

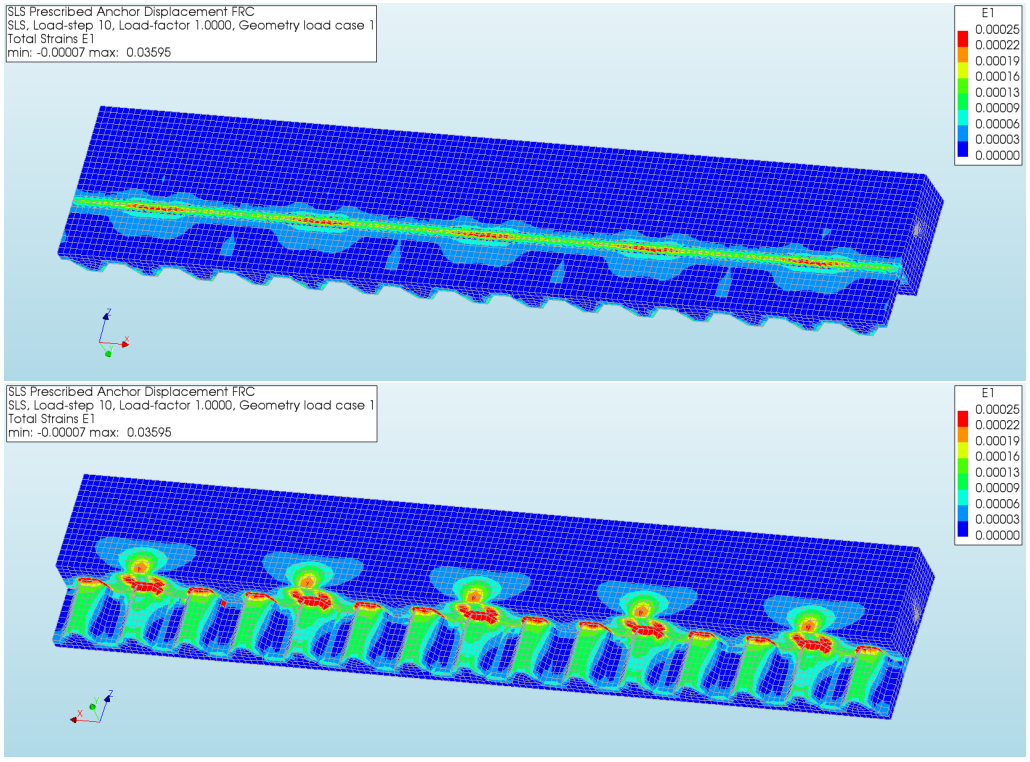

Figure E.2: *Total Strain in service limit state, front and back of capping beam for fiber reinforced concrete.*

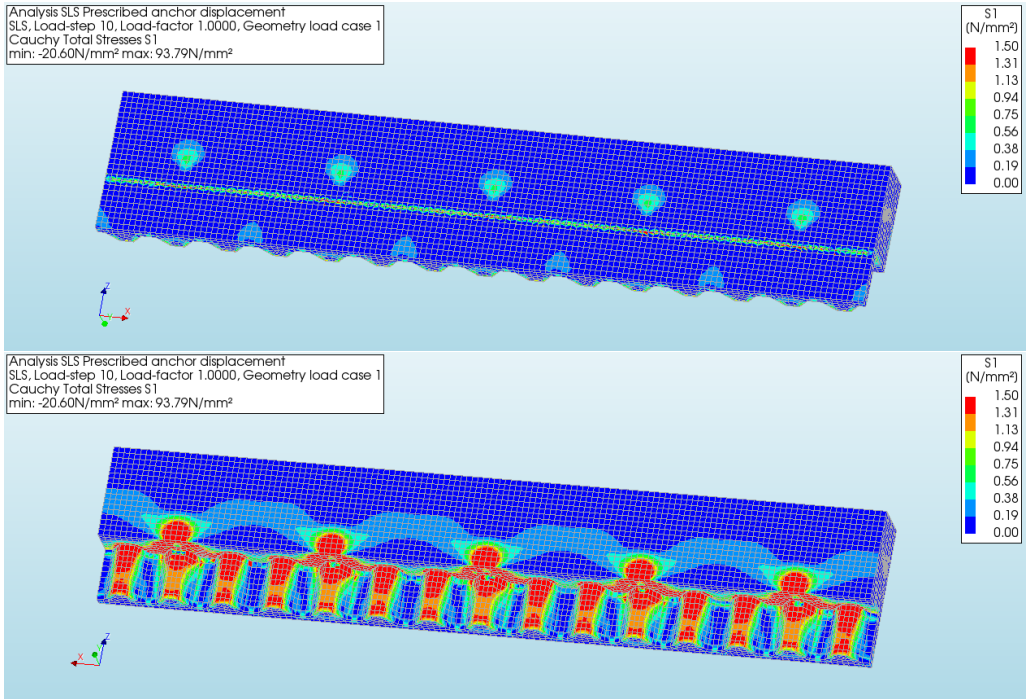

Figure E.3: *Principal stress in service limit state, for front and back of capping beam, conventionally reinforced concrete.*

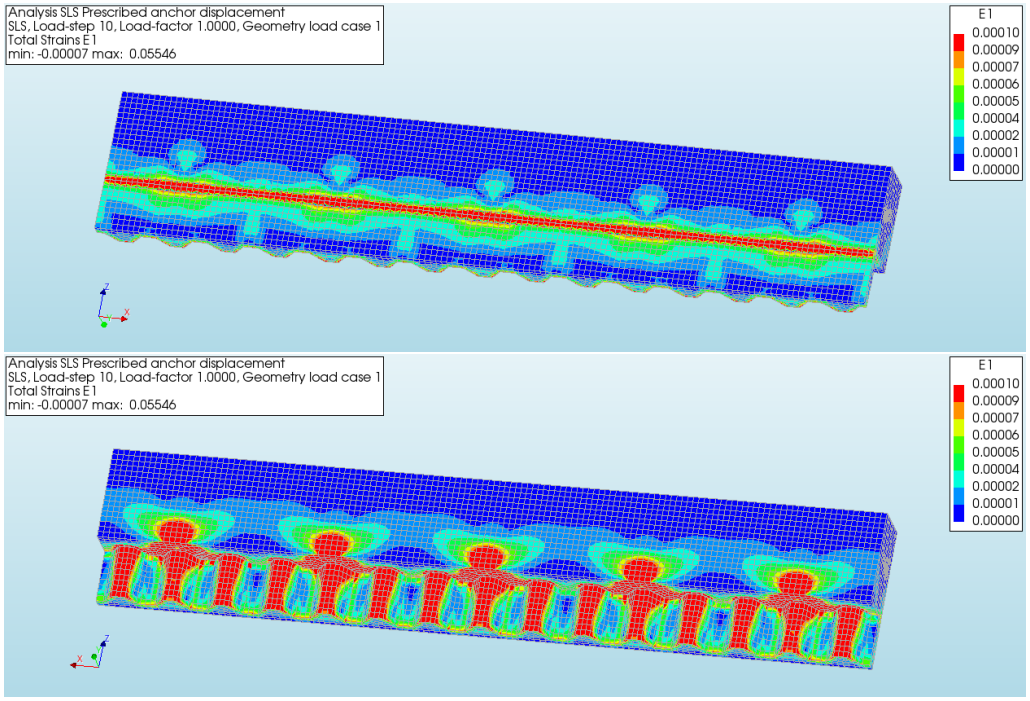

Figure E.4: *Total Strain in service limit state, front and back of capping beam for conventionally reinforced concrete.*

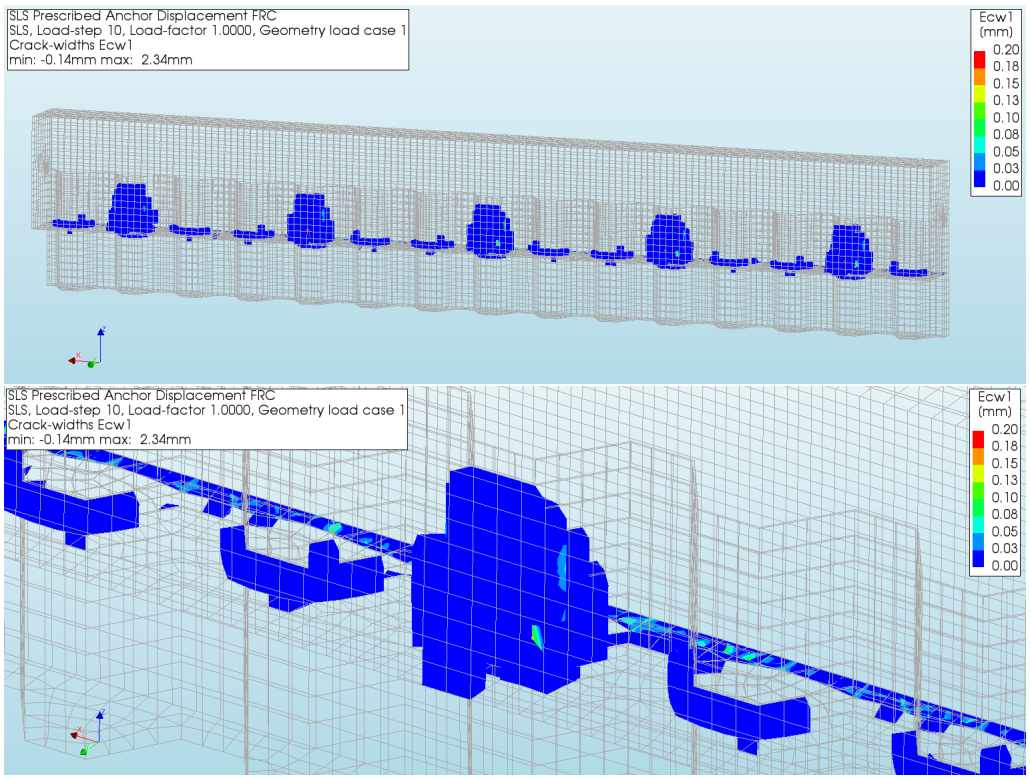

Figure E.5: *Crack widths formed in serviceability limit state for fiber reinforced concrete. Limit set to 0.2 mm as the permitted crack width.*

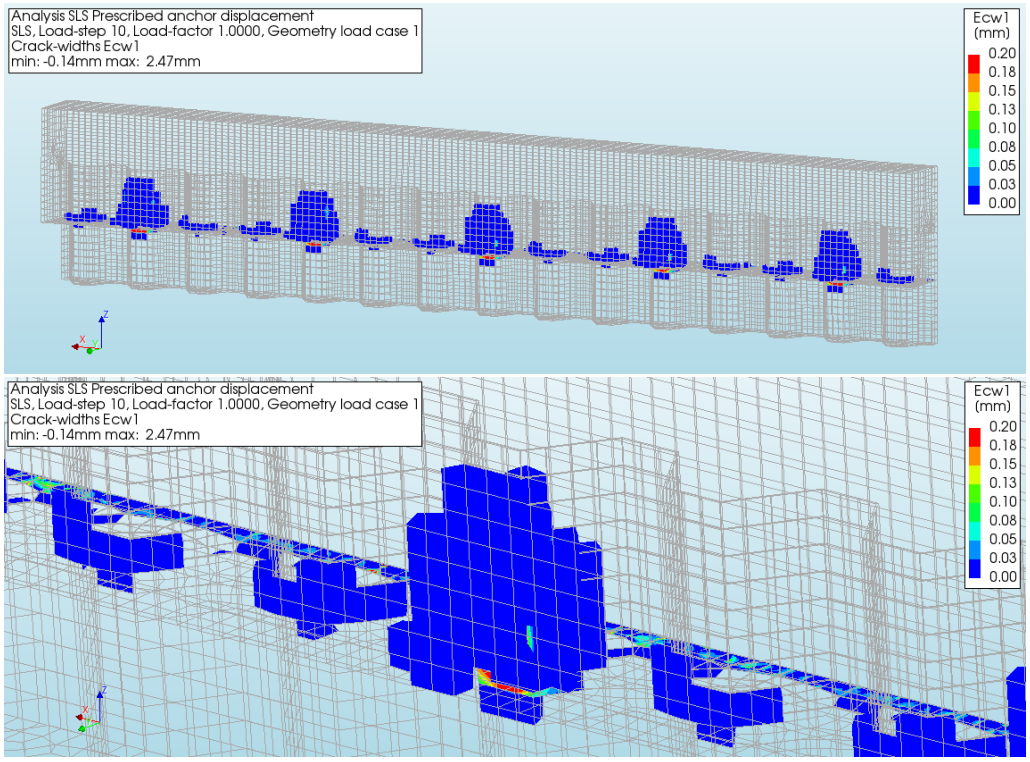

Figure E.6: *Crack widths formed in serviceability limit state for conventionally reinforced concrete. Limit set to 0.2 mm as the permitted crack width.*

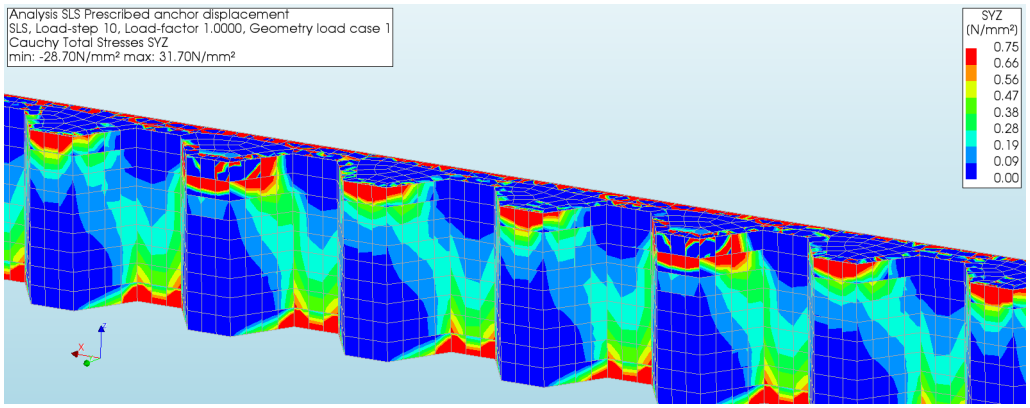

Figure E.7: *Shear stress of capping beam extension in service limit state for conventionally reinforced concrete. Limit set to 0.75 MPa in* S_{YZ}.

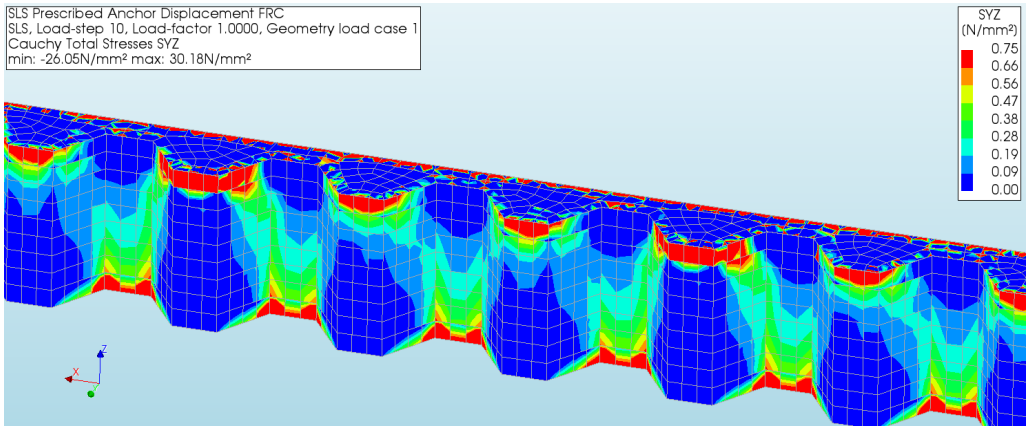

Figure E.8: *Shear stress of capping beam extension in service limit state for fiber reinforced concrete. Limit set to 0.75 MPa in* S_{YZ}.

F

Appendix F

Crack strains in the conventionally reinforced capping beam can be seen in Figure F.1, while principal stresses can be seen in Figure F.2.

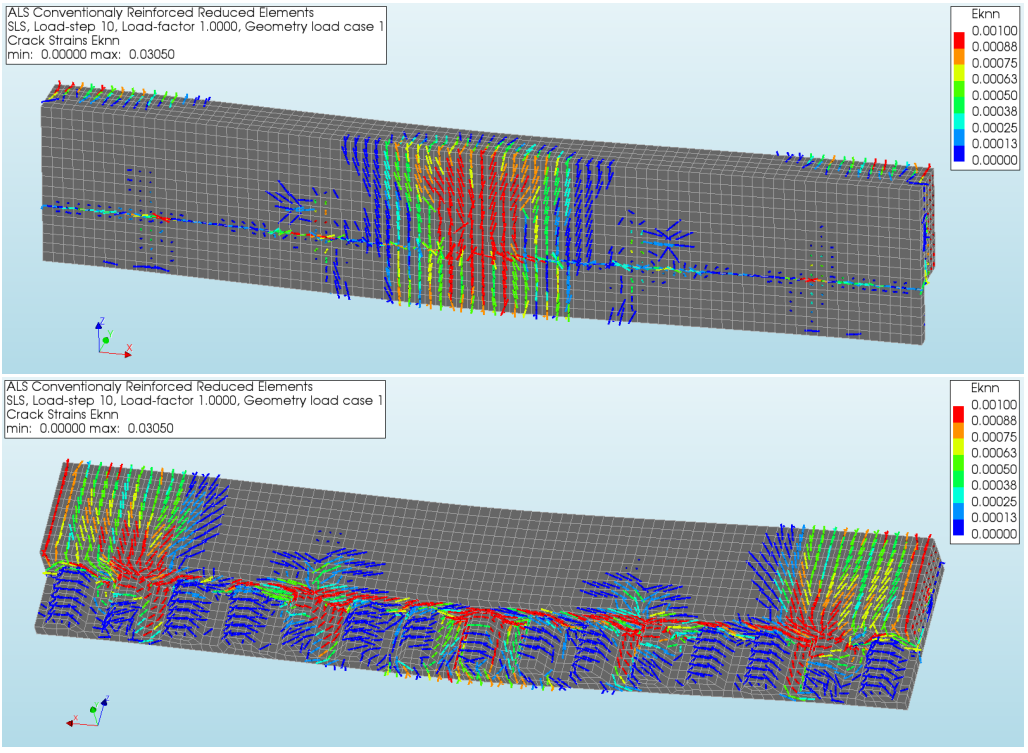

Figure F.1: *Crack strains in accidental limit state for conventionally reinforced concrete.*

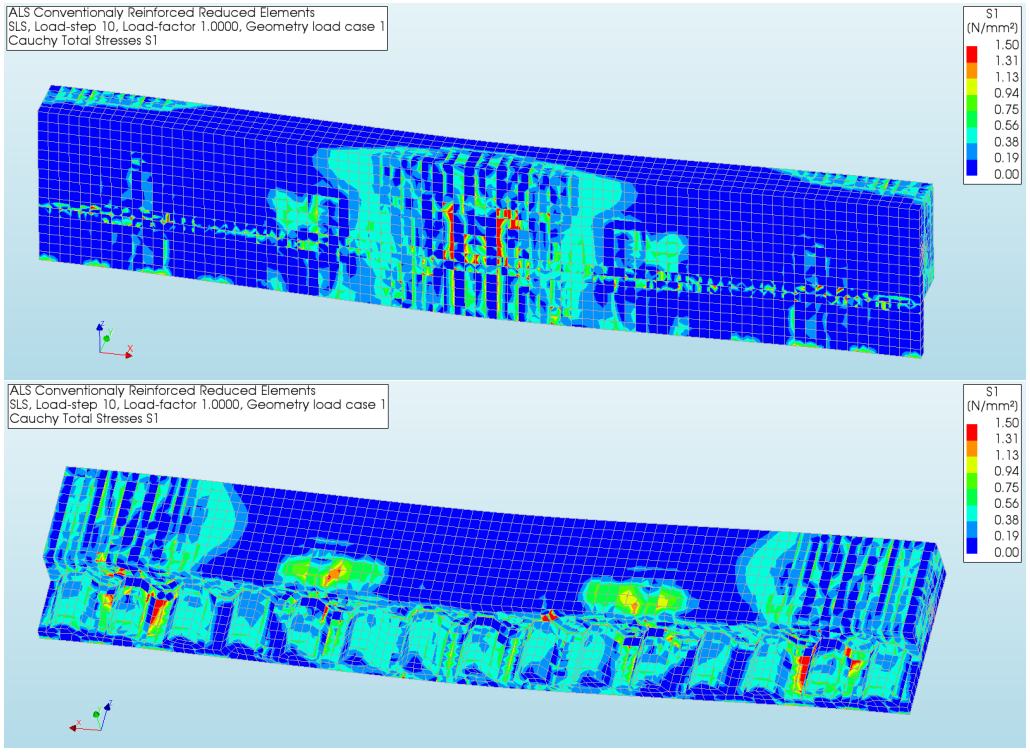

Figure F.2: *Principal stress in accidental limit state for conventionally reinforced concrete. Maximum value, 2.0 MPa*

G

Appendix G

$L := 4.2m$ Span length. Length between anchors

$F := 371kN$ Reaction force in SLS

$\varphi := 1.5$ Creep factor

$q := \frac{F}{L} = 88.333 \cdot \frac{kN}{m}$ Distributed load

$E_{concrete} := \frac{34}{1 + \varphi} GPa = 13.6 \cdot GPa$

$M_{support} := 0.0714 \cdot q \cdot L^2 = 111.255 \cdot kN \cdot m$ Moment over supports

$M_{span} := 0.0364 \cdot q \cdot L^2 = 56.718 \cdot kN \cdot m$ Moment over in mid span

Beam width

$b := 350mm$

Beam height

$h := 840mm$

$I := \frac{b \cdot h^3}{12} = 0.017 m^4$ Moment of inertia of considered cross-section geometry

$\sigma_{span} := \frac{M_{span}}{I} \cdot \frac{h}{2} = 1.378 \cdot MPa$ Maximum stress in mid span

$\sigma_{support} := \frac{M_{support}}{I} \cdot \frac{h}{2} = 2.703 \cdot MPa$ Maximum stress over supports

prescribed

Strains

$\varepsilon_{span} := \frac{\sigma_{span}}{E_{concrete}} = 1.013 \times 10^{-4}$

$\varepsilon_{spanDiana} := 1.0 \cdot 10^{-4}$

$\varepsilon_{support} := \frac{\sigma_{support}}{E_{concrete}} = 1.988 \times 10^{-4}$

$\varepsilon_{supportDiana} := 1.4 \cdot 10^{-4}$

Strain differences hand. cal vs. Diana

$\Delta_{span} := \frac{\varepsilon_{span} - \varepsilon_{spanDiana}}{\varepsilon_{span}} = 0.013$

$\Delta_{support} := \frac{\varepsilon_{support} - \varepsilon_{supportDiana}}{\varepsilon_{support}} = 0.296$

Figure G.1: *Hand calculations for comparison of stresses and strains in concrete.*